

# Perceptual Deep Depth Super-Resolution

Oleg Voinov<sup>1</sup>, Alexey Artemov<sup>1</sup>, Vage Egiazarian<sup>1</sup>, Alexander Notchenko<sup>1</sup>,  
Gleb Bobrovskikh<sup>1,2</sup>, Denis Zorin<sup>3,1</sup>, Evgeny Burnaev<sup>1</sup>

<sup>1</sup>Skolkovo Institute of Science and Technology, <sup>2</sup>Higher School of Economics,  
<sup>3</sup>New York University

{oleg.voinov, a.artemov, vage.egiazarian, alexandr.notchenko}@skoltech.ru,  
bobrovskikh@gmail.com, dzorin@cs.nyu.edu, e.burnaev@skoltech.ru

## Abstract

RGBD images, combining high-resolution color and lower-resolution depth from various types of depth sensors, are increasingly common. One can significantly improve the resolution of depth maps by taking advantage of color information; deep learning methods make combining color and depth information particularly easy. However, fusing these two sources of data may lead to a variety of artifacts. If depth maps are used to reconstruct 3D shapes, e.g., for virtual reality applications, the visual quality of upsampled images is particularly important. The main idea of our approach is to measure the quality of depth map upsampling using renderings of resulting 3D surfaces. We demonstrate that a simple visual appearance-based loss, when used with either a trained CNN or simply a deep prior, yields significantly improved 3D shapes, as measured by a number of existing perceptual metrics. We compare this approach with a number of existing optimization and learning-based techniques.

## 1. Introduction

RGB-D images are increasingly common as sensor technology becomes more widely available and affordable. These images can be used to reconstruct the 3D shapes of objects as well as their surface appearance. The better the quality of the depth component, the more reliable the reconstruction.

Unfortunately, for most methods of depth acquisition, the resolution and quality of the depth component are significantly lower than that of the RGB component. As there is a high correlation between the geometric features of the color image and the depth map (e.g., object edges), it is natural to use the color image to improve the resolution of the depth map.

A critical aspect of any upsampling method is the measure of quality it optimizes (i.e., the loss function), whether the technique is data-driven or not. While the choice is in

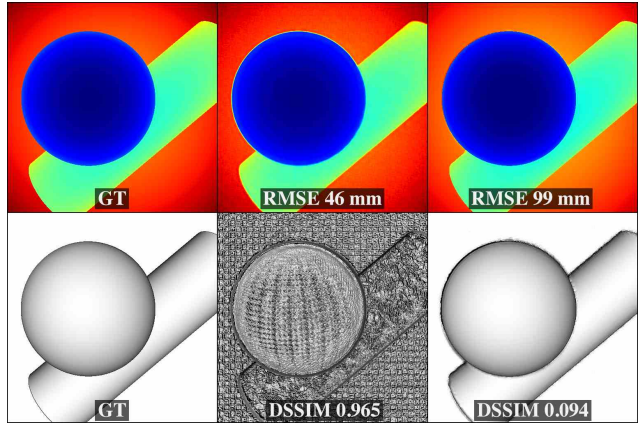


Figure 1: Depth-maps at the top and surface renderings at the bottom for the ground-truth on the left and super-resolution results, given by two different methods, in the middle and on the right. Visually inferior result gets higher score according to RMSE applied to depth directly but lower score according to DSSIM perceptual metric applied to rendered image of the 3D surface. Notice that the depth maps look almost identical while the corresponding rendered images differ significantly.

general application-dependent, many problems share similar criteria for the choice of a quality measure.

In this paper, we focus on applications that require reconstruction of 3D geometry visible to the user (e.g., acquisition of realistic 3D scenes for virtual or augmented reality and computer graphics). In this case, the *visual* appearance of the resulting 3D shape is of particular importance, i.e., how the surface looks when observed under various lighting conditions.

Most existing research on depth super-resolution is dominated by simple measures based on the direct comparison of pointwise depth values, (e.g., RMS error between two depth maps). However, the pointwise difference in depth does not capture the visual difference between two simi-

lar 3D shapes at a given location (*c.f.* Figure 1): *e.g.*, low-amplitude high-frequency variations of depth in some location may correspond to a significant difference in appearance; conversely, relatively large smooth changes in depth may be perceptually less relevant.

In this paper, we explore super-resolution of depth maps using a loss function based on visual differences. We propose to compare the rendered images of the surface (see Figure 1) instead of depth values directly. Our loss function can be computed efficiently and is shown to be highly correlated with more elaborate perceptual metrics. We demonstrate that this simple idea results in a dramatic improvement of visual quality, when used in two neural network-based RGB-D superresolution algorithms.

We compare our results to six state-of-the-art methods of depth super-resolution, based on distinct principles and using several types of loss functions, using perceptual metrics and an informal perceptual study.

In summary, our contributions are as follows:

- We demonstrate that a simple and efficient perceptually-motivated metric for depth-image comparison can be, on the one hand, easily combined with neural network-based whole-image upsampling techniques, and, on the other hand, is correlated with established proxies for human perception, validated w.r.t. experimental measurements;
- We demonstrate with extensive comparisons that, with the use of this metric, two methods for depth-image upsampling, one based on trainable CNN and the other based on the deep prior, yield high-quality results as measured by multiple perceptual metrics.

Throughout the paper we use *depth map* to refer to the depth component of an RGBD image, and *normal map* to refer to the map of the same resolution with a 3D surface normal direction computed from the depth map at each pixel. Finally, the *rendering of a depth map* refers to the grayscale image obtained by constructing a 3D triangulation of the height field represented by the depth map, computing the normal map from this triangulation, and rendering it using fixed material properties and a choice of lighting. This is distinct from commonly used depth map visualizations using grayscale values obtained from the depth map values by simple scaling. We describe this in more detail in Section 3.

## 2. Related work

### 2.1. Metrics for depth map differences

Metrics play two important roles in the works on image super-resolution, inpainting, enhancement, and related topics: on the one hand, they are used to formulate an optimization functional or a loss function; on the other hand, they are used to evaluate the quality of the results. Ideally, these should be the same; however, in some instances, this

is not the case. In the former case, the efficiency of evaluation and differentiability are significant considerations; in the latter, the top priority is to capture the needs of the application.

In most works on depth map reconstruction and upsampling, a limited number of simple metrics are used, both for optimization and final evaluation. Typically these are scaled  $L_2$  ((R)MSE) or  $L_1$  norm of the differences in depth (*e.g.*, [9, 19]).

Another set of measures introduced in [20] and primarily used for evaluation, not optimization or learning, are heuristic measures of various aspects of the depth map geometry: foreground flattening/thinning, fuzziness, bumpiness, etc. Most of them require a very specific segmentation of the image: *e.g.*, detection of flat areas and depth discontinuities.

Visual similarity metrics aim to be consistent with human judgment, *e.g.*, in the sense of similarity ordering (which of two images is more similar to the ground truth?). Well-established visual metrics include those based on simple vision models of *structural similarity*: SSIM [51], FSIM [58], MSSIM [52]. We discuss SSIM in greater detail in Section 3. A different metric is presented in [35]. It is based on a sophisticated model of low-level visual processing. Recently, a number of perceptually-based metrics produced by neural nets were proposed (see [59] for a detailed overview). These metrics use a simple distance measure (*e.g.*,  $L_2$ ) on deep features learned for, *e.g.*, a classification task. They were demonstrated to outperform statistical measures such as SSIM.

### 2.2. Depth super-resolution

Depth super-resolution is closely related to a number of other tasks performed on depth maps: in particular, denoising, enhancement, inpainting, and densification (see, *e.g.*, [5, 6, 34, 21, 8, 33, 46, 55]).

We focus on works addressing the super-resolution problem directly. More specifically, we review methods for estimation of high-resolution depth map from a single low-resolution depth map and a high-resolution RGB image.

**CNNs.** Among learning-based methods, convolutional neural networks have achieved impressive performance in high-level computer vision tasks and recently have been applied to depth super-resolution.

Most of the research on single depth map super-resolution using CNNs has been within the RGB-D framework [30, 43, 53, 39], as depth and color information is easy to combine in typical CNN architectures. The hybrid method of [39, 43] add subsequent optimization stages to a CNN to produce sharper results. The method [22] follows a similar approach: it resolves ambiguity in the low-resolution depth map upsampling by adding high-frequency features from high-resolution RGB data. Other approaches to CNN-based photo-guided depth super-resolution include linear filtering with CNN-derived kernels [26], deep fusion

of time-of-flight depth and stereo images [1], and a method based on generative adversarial networks [63].

All of these techniques use either  $L_2$  or  $L_1$  norm of the depth differences as the basis of their loss functions, often combined with regularizers of different types. The closest to our approach is [63], which includes the difference of gradients as one of the loss function terms, which captures some of the visual information.

For evaluation, all methods report RMS or PNSR metric on depth differences and/or mean absolute error of depth differences. In addition, [4, 44, 63, 43] report the perceptual metric SSIM *also applied directly to depth maps, rather than depth map renderings*.

**Dictionary learning** has been investigated for depth super-resolution, with some representative approaches being [11, 13, 29]. However, dictionary learning is typically restricted to small dimensions and as a result to structurally simpler depth maps, compared to CNNs.

**Variational approach.** Variational approaches aim to combine RGB and depth information explicitly by carefully designing an optimization functional, without relying on learning. Most relevant examples are shape-from-shading optimization to improve single-image depth super-resolution [14], combining reflectance map estimation with multiple-image depth super-resolution [38]. Some of these methods include visual metric-related terms in the functional, and [38] includes normal comparison in the evaluation, capturing visual similarity.

While showing impressive results in many cases, these methods typically require prior segmentation of foreground objects and depend heavily on the quality of such segmentation. Another strategy to tackle ambiguities in super-resolution is to design sophisticated regularizers to balance the data-fidelity terms against a structural image prior [15, 24, 56]. In contrast to such approaches, which require custom hand-crafted regularized objectives and optimization procedures, we focus on the standard training strategy (*i.e.*, gradient-based optimization of a CNN) while using a loss that captures visual similarity.

A less common, but promising strategy is to leverage multiple frames of RGB-D video for high-resolution depth estimation [45]. While we do not consider this setting in our work, we expect that it can be extended to this problem. Yet another approach is to choose a carefully-designed model such as [64] featuring a sophisticated metric defined in a space of minimum spanning trees and including an explicit edge inconsistency model. Compared to our approaches, such models require manual tuning of multiple hyperparameters.

### 2.3. Perceptual photo super-resolution

Perceptual metrics were considered more broadly in the context of image super-resolution. A number of CNN-based methods provide accurate 2D image super-resolution, evaluated in terms of MSE [60, 16, 61, 18]. However, it was observed that MSE is not always correlated with perceptual



Figure 2: Depth map renderings with light directions that we use to calculate the perceptual metrics.

quality. In [25] the authors optimize  $L_2$  loss on the deep features. To improve further those results the authors of [28] besides using a similar perceptual metric, used an adversarial loss to push the SR solution to the natural image manifold using a discriminator network. Instead of using a perceptual loss, [36] and subsequent works [50, 57, 12] proposed to consider the distribution of features in an image and train the network to generate images with natural feature distributions for SR. To balance between the perceptual quality and MSE of SR, [31] and [7, 49] proposes to use GAN architectures. In [32] the authors conducted human subject studies using a large set of super-resolution images and proposed a metric learned from visual perceptual scores. However, the article [62] discusses their convergence properties and claims that poor performance of some losses is related to local minima of the loss functions.

## 3. Metrics

In this section, we discuss visually-based metrics and how they can be used both to evaluate the quality of depth map super-resolution and as loss functions. The general principle we follow is to apply comparison metrics to *renderings* of the depth maps to obtain a measure of their difference, instead of considering depth maps directly. The difficulty with this approach is that there are infinitely many possible renderings depending on lighting conditions, material properties and camera position. However, we demonstrate that even a very simple rendering procedure already yields substantially improved results.

**From a depth map to a visual representation.** To approximate the appearance of a 3D scene depicted with a certain depth map, we use a simple rendering procedure. We illuminate the corresponding 3D surface with monochromatic directional light source and observe it with the same camera that the scene was originally acquired with. We use the diffuse reflection model and do not take visibility into account. For this model, the intensity of a pixel  $(i, j)$  of the rendering  $I$  is proportional to cosine of the angle between the normal at the point of the surface, corresponding to the pixel,  $\mathbf{n}_{ij}$  and the direction to the light source  $\mathbf{e}$ :  $I_{ij} = \mathbf{e} \cdot \mathbf{n}_{ij}$  (see Figure 2). Any number of vectors  $\mathbf{e}$  can be used to generate a collection of renderings representing the depth map. We observe however, that all of them can be obtained using a linear combination of any three independent light field directions. We consider three basic depth map renderings in an orthogonal basis  $\mathbf{e}_1, \mathbf{e}_2, \mathbf{e}_3$ .



First, we discuss key examples of standard perceptual metrics. While these can be potentially used also as loss functions, the choice of a loss function needs to take stability and efficiency into account, so we opt for a more conservative choice described below. We use underscore "d" for the metrics applied to depth directly, and underscore "v" for the metrics applied to rendered images or based on visual-differences.

**Perceptual metrics.** We briefly describe two representative metrics: a statistics-based SSIM (DSSIM), and a neural network-based LPIPS. Either of these can be applied to the three basis renderings (or a larger sample of renderings) and added together to obtain a complete metric. In the supplementary material, we describe some additional metrics that we have explored with similar outcomes in terms of relative performance of different superresolution methods.

*SSIM* [51] (structural similarity index measure) is a widely used metric that aims to take into account the changes in the local structure of an image, captured by a number of statistical quantities computed on a small window around each pixel. For each pixel, three terms – the luminance term  $\ell$ , the contrast term  $c$  and the structural term  $s$ , each normalized to be bounded by 1 – are computed using the local means  $\mu_1, \mu_2$ , standard deviations  $\sigma_1, \sigma_2$  and cross-covariance  $\sigma_{12}$  of corresponding local windows in two images  $I_1$  and  $I_2$ ,

$$\ell = \frac{2\mu_1\mu_2}{\mu_1^2 + \mu_2^2}, \quad c = \frac{2\sigma_1\sigma_2}{\sigma_1^2 + \sigma_2^2}, \quad s = \frac{\sigma_{12}}{\sigma_1\sigma_2},$$

The SSIM value is computed as mean per-pixel product of these three terms  $\text{SSIM}_v(I_1, I_2) = \frac{1}{N} \sum_{ij} \ell_{ij} \cdot c_{ij} \cdot s_{ij}$ . We use "the lower – the better" structural dissimilarity index measure computed as  $\text{DSSIM}_v(I_1, I_2) = 1 - \text{SSIM}_v(I_1, I_2)$ .

*Neural net-based metrics.* The overall underlying idea of all of these metrics is to compute an  $L_2$  distance between features extracted from a neural network. Specifically, for each of the compared images  $I_k$ ,  $k \in \{1, 2\}$ , features  $x_{k\ell}$ ,  $\ell = 1 \dots L$ , are extracted from  $L$  layers of the network (with different  $L$  for each network type). If  $\ell$ -th layer feature map is of dimension  $H_\ell \times W_\ell \times C_\ell$ , where  $H_\ell$  and  $W_\ell$  are spatial dimensions and  $C_\ell$  is the number of channels, then, in the simplest case, the error is computed as

$$\text{NN}_v(I_1, I_2) = \sum_\ell \frac{1}{H_\ell W_\ell} \sum_{ij} \|\hat{x}_{1\ell,ij} - \hat{x}_{2\ell,ij}\|_2^2,$$

where the "hat" symbol denotes unit normalization of feature vectors along the channel dimension. We use the *Learned Perceptual Image Patch Similarity* (LPIPS), proposed in [59], which applies a learned channel-wise weighting in addition to the formula above, and the corresponding choice of networks: Alexnet [27], VGG [41] (5 layers are used from both), and SqueezeNet [23] (the first layer is used).

**Our visual difference-based metric.** While the perceptual metrics described above are good proxies for human evaluation of differences between depth map renderings, they are

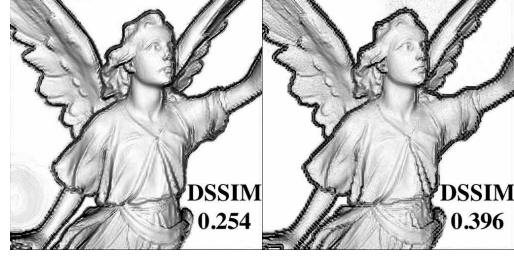


Figure 3: Results of DIP optimization using our loss on the left and DSSIM loss on the right with the corresponding values of DSSIM metric. Note that the metric values here are calculated for the rendering conditions corresponding to these images in contrast to the worst values in Section 5.

lacking as loss functions, due to their complex landscapes. For example, DSSIM metric when used as a loss, produces results that are actually inferior with respect to the *DSSIM metric itself* compared to a simpler loss function we define below (Figure 3).

The LPIPS metric has complex energy profile typical for neural nets, and having a neural net as a part of the loss function for another may behave unpredictably.

The simplest metric capturing differences between depth map renderings of  $d_1$  and  $d_2$  can be computed simply as the square root of averaged squared differences between three basis renderings  $e_m \cdot n_1$  and  $e_m \cdot n_2$ ,  $m = 1, 2, 3$ :

$$\text{RMSE}_v(d_1, d_2) = \sqrt{\frac{1}{N} \sum_{i,j,m} \|e_m \cdot n_{1,ij} - e_m \cdot n_{2,ij}\|_2^2},$$

where indices  $i, j$  enumerate  $N$  pixels of the image. We observe that for orthonormal directions  $e_m$ , this is equivalent to the RMS difference of the normal maps of two images.

We found that this simple metric for depth map comparison is efficient and stable, and at the same time we demonstrate in Section 5 that (at least for depth maps) it is correlated with DSSIM and LPIPS, *i.e.*, situations when one metric has high values and the other has low values are unlikely. Our experiments confirm that optimizing this metric also reduces both perceptual metrics.

## 4. Methods

We have selected eight representative methods based on different principles, which, based on the literature, are state-of-the-art in their categories: (1) a purely variational method [14]; (2) a bilateral filtering method, using a high-resolution edge map [54]; (3) a dictionary learning method [13]; (4) a hybrid CNN-variational method [39]; (5) a pure CNN method [22]; (6) a zero-shot CNN method [47]; (7) a densification [34] and an enhancement [55] neural network-based methods.

Our goals are (a) to modify the methods to use the visual difference-based loss function, (b) to compare the results of the enhanced methods with alternatives of different types.



Our experiments showed that algorithms [34] [55], do not perform well compared to others, and so we did not consider them.

We found that two neural network-based methods (5) and (6) can be easily modified to use a visual difference-based loss functions, as we explain in more detail now.

We combine our visual difference-based metric (without square root) with mean absolute deviation on Laplacian pyramid  $\text{Lap}_1$  (see [2]) as a regularizer:

$$\mathcal{L}(d_1, d_2) = \text{Lap1}(d_1, d_2) + w \cdot \text{MSE}_v(d_1, d_2) \quad (1)$$

and use this function as the replacement for  $\text{MSE}_d$ . We modify two algorithms, which we refer to as MSG and DIP. **MSG** [22] is a carefully-designed state-of-the-art deep learning architecture, that uses different strategies to upsample different spectral components of low-resolution depth map. We denote the modified version of this method with visual difference-based loss by **MSG-V**.

**DIP** [47] is a zero-shot deep learning approach, based on a remarkable observation that, even without any specialized training, the structure of CNN itself may be leveraged for solving inverse problems on images. We note that this approach naturally allows simultaneous super-resolution and inpainting. However, originally, the super-resolution problem is formulated for one-channel image:

$$d^{\text{SR}} = \text{CNN}_{\theta^*}, \quad \theta^* = \arg \min_{\theta} \text{MSE}_d(\mathbf{D}(\text{CNN}_{\theta}), d^{\text{LR}}),$$

where  $d^{\text{LR}}$  and  $d^{\text{SR}}$  are the low-resolution and super-resolved depth maps,  $\text{CNN}_{\theta}$  is the output of the used deep neural network parametrised by  $\theta$  and  $\mathbf{D}$  is the downsampling operator. To perform photo-guided super-resolution we modify the problem statement simply by adding an additional intensity output channel to the neural network:

$$d^{\text{SR}} = \text{CNN}_{\theta^*}^{(1)}, \quad \theta^* = \arg \min_{\theta} \text{MSE}_d(\mathbf{D}(\text{CNN}_{\theta}^{(1)}), d^{\text{LR}}) + \text{Lap1}(\text{CNN}_{\theta}^{(2)}, I^{\text{HR}}),$$

where  $I^{\text{HR}}$  is the high-resolution photo-guidance and the corresponding term of the loss is mean absolute deviation on Laplacian pyramid (see [2]). We denote the version of this method with  $\text{MSE}_d$  replaced with visual difference-based loss by **DIP-V**.

We use the remaining four methods (1)-(4) for comparison as-is, as modifying them to use a different loss function would require substantial changes to the algorithms.

**SRfS** [14] is a state-of-the-art method relying on a combined variational formulation of super-resolution and shape-from-shading problems. It already includes a visual-difference based term (the remaining methods use depth difference metrics). **EG** [54] is a depth-only MRF-based approach combining depth upsampling with prediction of smooth high-resolution edges. It does not use a loss directly, thus cannot be easily adapted. **DG** [13] is a depth map enhancement method based on dictionary learning, capable of simultaneous super-resolution and inpainting, us-

ing depth difference-based fidelity term. It makes a number of modeling choices which may or may not be suitable for a different loss function, and typically does not perform as well as neural network-based methods. **PDN** [39] is a hybrid method featuring two stages: the first is composed of fully-convolutional layers and predicts a rough super-resolved depth map, and the second performs an unrolled variational optimization, aiming to produce a sharp and noise-free result.

## 5. Experiments

### 5.1. Data

For evaluation, we select a representative and diverse set of 34 RGB-D images featuring synthetic and real data, both with different levels of geometry and texture complexity, including low- and high-quality real data. We employ four datasets, most commonly used in literature on depth super-resolution, and our SimGeo dataset. *SimGeo* is a synthetic dataset created with Blender that consists of 6 simple scenes with and without low- and high-frequency textures. The purpose of *SimGeo* examples is to clearly show artifacts that are not related to the noise or high-frequency geometry in the input data. We also use it to explore to what extent using RGB inputs with color variation on smooth surfaces for depth superresolution produces false geometric detail.

*ICL-NUIM* [17] includes photo-realistic RGB images along with synthetic depth, free from any acquisition noise. *Middlebury 2014* [40] is captured with a structured light system for complex real-world scenes and provides high-quality ground truth. For our evaluation, we select samples of different complexity in geometry and texture.

*SUN RGB-D* [42] contains RGB-D images captured with four different consumer-level RGB-D cameras, including Intel RealSense, Asus Xtion, Microsoft Kinect v1 and v2. *ToFMark* [10] is a challenging real-world benchmarking dataset providing real time-of-flight and intensity camera acquisitions together with an accurate ground truth, measured using a structured light sensor. For additional details on our evaluation data please refer to supplementary material.

We generate low-resolution inputs for the scaling factors of 4 and 8, that are most common among the works on depth super-resolution. We employ two downsampling models, most commonly used in the literature on depth super-resolution: Box downsampling, *i.e.*, each low-resolution pixel contains mean value over the “box” of  $s \times s$  high-resolution neighbouring pixels, where  $s$  is the scaling factor, and Nearest neighbour downsampling, *i.e.*, each low-resolution pixel contains the value of the nearest high-resolution pixel.

### 5.2. Evaluation details

For evaluation of the methods SRfS, EG, DG and MSG we use the code and pretrained models provided by the au-

thors<sup>1</sup>. For evaluation of PDN, we use the publicly available code to train the model. We adapt publicly available implementation of DIP for depth maps, as described in Section 4 and evaluate this adaptation with original MSE loss and our visual-difference-based loss. We reimplement MSG on PyTorch [37] to train it with visual-difference-based loss and train it according to the original paper on patches collected from Middlebury and MPI Sintel [3] datasets. We choose the weighting parameter  $w$  in Equation (1) so that both terms of the loss contribute equally in terms of magnitude (see supplementary material for more details).

For each super-resolution result, we measure different pixel-wise metrics applied directly to depth maps and different perceptual metrics on depth map renderings. For calculation of perceptual metrics, we render the depth map with three orthogonal light directions (the first three in Figure 2) and one additional light direction (the mean over these three). We use the worst values over the four light directions and visualize the results using the last one. The complete set of visualizations is available online<sup>2</sup>; for the complete set of metric values please refer to supplementary material.

Additionally, we conducted an informal perceptual study using the results calculated on SimGeo, ICL-NUIM and Middlebury datasets, in which a subject was asked to choose the renderings of the upsampled depth maps that look most similar to the ground truth image.

### 5.3. Evaluation of metrics

We explore correlations between several metrics used in loss functions of superresolution algorithms and some perceptual metrics. In [59], neural net-based perceptual metrics, LPIPS in particular, are experimentally shown to represent human perception well. For this reason, we use their values as the reference for other metrics. Specifically, we consider RMSE, BadPix and Bumpiness metrics applied to depths directly, same metrics applied to the depth map renderings as in our loss function, DSSIM and LPIPS metrics applied to depth map renderings.

For each pair of metrics we calculate the Pearson correlation coefficient. We find that metrics applied to depth directly, demonstrate weak correlation with perceptual metrics on applied to depth map renderings (see Figure 4 for several examples, and a complete set in the supplementary material) and are not suitable for predicting visual quality of depth super-resolution results. For example, consider RMSE<sub>d</sub> values in Table 1 for the results with the worst visual quality in Figure 5). On the other hand, our RMSE<sub>v</sub> correlate well with the perceptual metrics, to the same extent they correlate between each other.

<sup>1</sup>For EG there is no publicly available pretrained model for x8.

<sup>2</sup><https://mega.nz/#F!yvRXBABI!pucRoBvtntzhzHIloqsxEvA!y6JmCajS>

### 5.4. Comparison of super-resolution methods

In Table 1 and Figure 5 we compare the super-resolution methods on our SimGeo dataset for the scaling factor of 4; in Table 2 and Figure 6 we compare the methods on ICL-NUIM and Middlebury datasets for the scaling factors of 4 and 8. The downsampling model used in both comparisons is *box*. For additional results, please refer to supplementary material. The methods EG, PDN and DG do not recover fine details of the surface, typically producing results inferior to bicubic upsampling with respect to visual quality measures. The methods SRfS and DIP suffer from false geometry artifacts for images of textured surfaces, and produce noisy surfaces. MSG also amplifies the noise in some surface regions. All methods from prior work, including those performing inpainting, namely, SRfS, DG and DIP perform relatively poorly on data with missing depth information (rendered in black). The EG method failed to converge.

In contrast, observe that integration of visual difference-based loss into DIP and MSG significantly improves the results of both methods qualitatively and quantitatively. The visual difference-based version of DIP do not suffer from false geometry artifacts due to color textures in input images compared to the original MSE<sub>d</sub> version. On the challenging Middlebury data, where it performs simultaneous super-resolution and inpainting, DIP-V mostly outperforms other methods as measured by the perceptual metrics and is preferred by more than 80% of subjects in the perceptual study. The visual difference-based version of MSG, although still struggling with "holey" data, in comparison to the original MSE<sub>d</sub> version, produces significantly less noisy results, almost without visual artefacts as compared to the other methods. On the data without missing measurements, including hole-filled Middlebury Vintage, MSG-V mostly outperforms other methods as measured by the perceptual metrics and is preferred by more than 80% of subjects. On SimGeo, ICL-NUIM and Middlebury combined, one of the visual difference-based versions of methods is preferred over the other methods by more than 85% of subjects.

For comparison, Figure 5 shows pseudo-color images, commonly used to visualize depth maps directly. Note that upsampled depth maps obtained with different methods are almost indistinguishable in these visualizations while the depth map renderings in the row below may be dramatically different.

## 6. Conclusions

Using a range of synthetic and real data we have demonstrated that using a visual difference-based metric for depth images as a loss function in CNN-based methods for depth map upsampling yields significantly better results in comparison to the approach based on direct pixel-wise depth deviations. Our metric and learning architectures are relatively simple, and we expect that this approach to definition

	Sphere and cylinder, x4				Lucy, x4				Cube, x4				SimGeo average, x4			
	RMSE <sub>d</sub>	DSSIM <sub>v</sub>	LPIPS <sub>v</sub>	RMSE <sub>v</sub>	RMSE <sub>d</sub>	DSSIM <sub>v</sub>	LPIPS <sub>v</sub>	RMSE <sub>v</sub>	RMSE <sub>d</sub>	DSSIM <sub>v</sub>	LPIPS <sub>v</sub>	RMSE <sub>v</sub>	RMSE <sub>d</sub>	DSSIM <sub>v</sub>	LPIPS <sub>v</sub>	RMSE <sub>v</sub>
SRfS [14]	70	887	1025	417	82	811	781	367	52	934	1036	361	61	711	869	311
EG [54]	55	143	326	130	69	357	426	220	43	113	214	105	53	168	306	136
PDN [39]	157	198	<u>295</u>	<u>150</u>	173	456	<u>368</u>	<u>251</u>	164	156	<u>250</u>	<u>145</u>	162	224	<u>278</u>	165
DG [13]	56	265	372	166	69	523	558	249	44	218	411	139	54	293	420	171
Bicubic	57	189	313	189	72	355	398	267	44	131	287	160	55	197	320	193
DIP [47]	46	965	1062	548	<u>53</u>	827	615	344	45	963	906	530	52	887	893	395
MSG [22]	41	626	859	229	54	444	480	259	29	445	687	176	39	374	569	194
DIP-V	<b>28</b>	560	766	142	<b>44</b>	421	446	223	<b>26</b>	352	613	146	<b>33</b>	313	524	147
MSG-V	99	<b>94</b>	<b>267</b>	<b>96</b>	74	<b>205</b>	<b>251</b>	<b>156</b>	102	<b>70</b>	<b>179</b>	<b>77</b>	96	<b>95</b>	<b>194</b>	<b>99</b>

Table 1: Quantitative evaluation on SimGeo dataset. RMSE<sub>d</sub> is in millimeters, other metrics are in thousandths. Lower values correspond to better results. The best result is in bold, the second best is underlined.

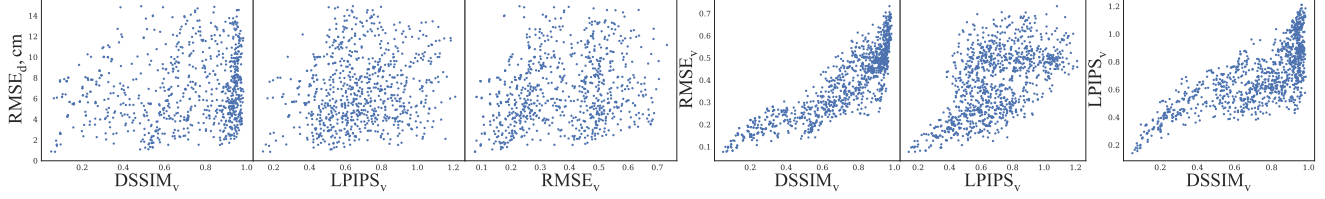


Figure 4: Scatter plots. Each point corresponds to one super-resolution result obtained with a certain method for a certain sample, downsampling model and scaling factor. The Pearson correlation coefficients are: 0.09, 0.05, 0.12, 0.85, 0.57, 0.75.

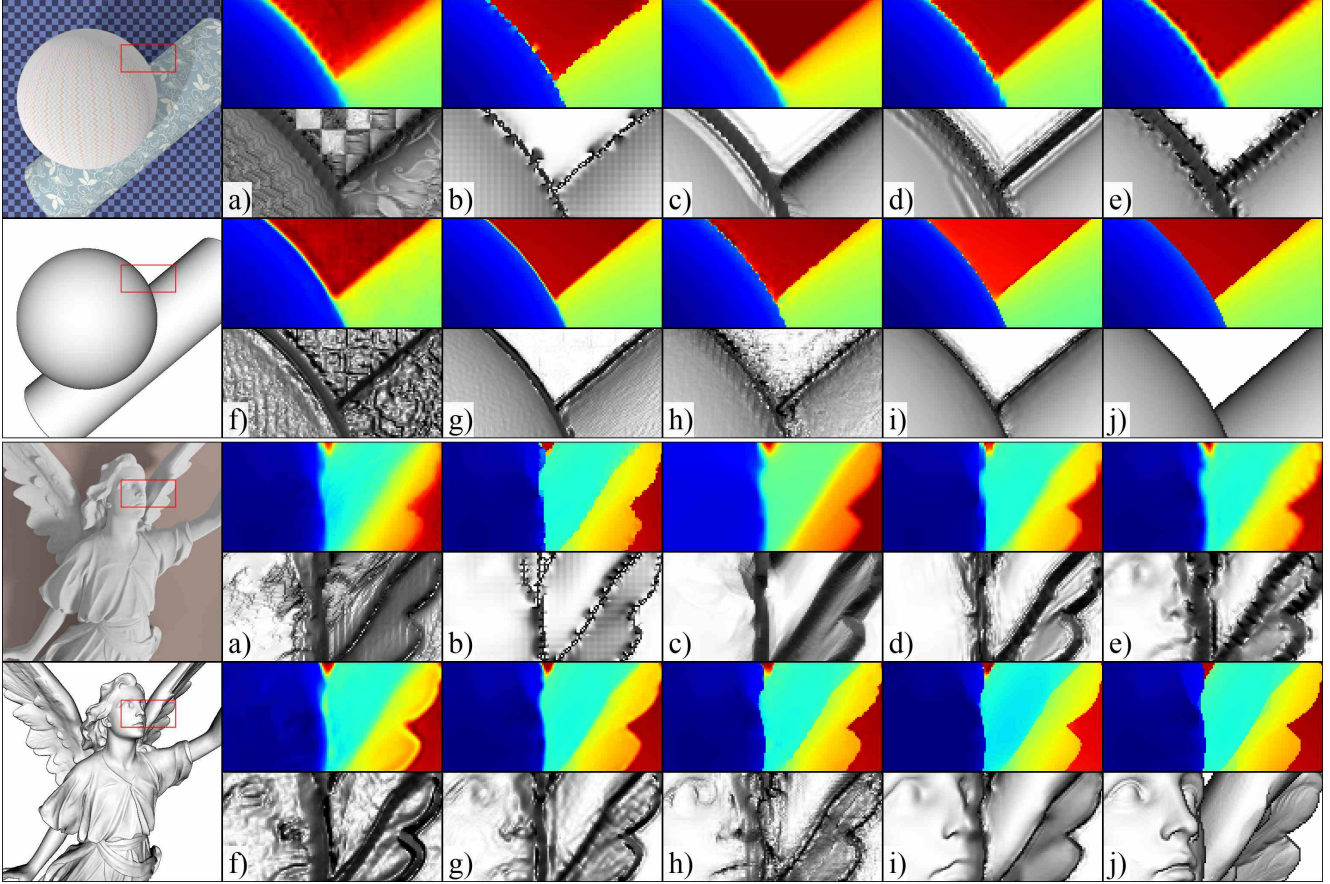


Figure 5: x4 super-resolution results on "Sphere and cylinder" and "Lucy" from SimGeo. Depth maps are in pseudo-color and depth map renderings are in grayscale. a) SRfS [14], b) Edge-Guided [54], c) PDN [39], d) DG [13], e) Bicubic, f) DIP, g) DIP-V, h) MSG [22], i) MSG-V, j) GT. Best viewed in color.



of loss functions will be beneficial for other related problems. In particular, combining these with inpainting methods to eliminate gaps may be promising.

We have focused on the case of single regularly sampled RGBD images, but a lot of geometric data has less regular form. Thus, the future work would be to adapt the developed methodology to the more general sampling of depth maps including multiple RGBD images and point clouds annotated with a collection of RGB images.

## **Acknowledgements**

The work was supported by The Ministry of Education and Science of Russian Federation, grant No. 14.615.21.0004, grant code: RFMEFI61518X0004.

The authors acknowledge the usage of the Skoltech CDISE HPC cluster Zhores for obtaining the results presented in this paper.

	Plant						Vintage						Recycle						Umbrella					
	DSSIM <sub>v</sub>		LPIPS <sub>v</sub>		RMSE <sub>v</sub>		DSSIM <sub>v</sub>		LPIPS <sub>v</sub>		RMSE <sub>v</sub>		DSSIM <sub>v</sub>		LPIPS <sub>v</sub>		RMSE <sub>v</sub>		DSSIM <sub>v</sub>		LPIPS <sub>v</sub>		RMSE <sub>v</sub>	
	x4	x8	x4	x8	x4	x8	x4	x8	x4	x8	x4	x8	x4	x8	x4	x8	x4	x8	x4	x8	x4	x8	x4	x8
SRfS [14]	658	692	632	649	280	309	721	749	631	<u>634</u>	346	382	715	772	610	623	376	410	843	853	797	831	397	443
EG [54]	568		677		255																			
PDN [39]	574	612	659	699	269	305	663	714	706	700	319	350	635	<b>701</b>	523	589	364	457	799	<b>828</b>	847	882	367	452
DG [13]	611	622	745	785	268	291	666	669	796	840	290	300	696	<u>719</u>	602	617	328	383	846	878	781	856	399	457
Bicubic	<u>562</u>	<u>610</u>	688	763	249	290	<u>558</u>	<u>649</u>	602	729	<u>258</u>	302	<b>575</b>	721	<u>474</u>	576	329	398	<b>749</b>	<u>837</u>	747	886	<u>323</u>	<u>380</u>
DIP [47]	919	880	764	723	490	437	953	965	910	872	656	687	871	923	576	605	434	500	915	953	737	<u>722</u>	467	528
MSG [22]	571	645	<u>582</u>	<b>495</b>	<u>234</u>	285	708	785	<b>510</b>	<b>610</b>	292	364	741	869	624	661	485	550	834	896	<u>678</u>	<u>787</u>	442	496
DIP-V	694	707	<b>463</b>	<u>555</u>	262	<u>276</u>	804	884	<u>579</u>	674	343	435	<b>575</b>	735	<b>388</b>	<b>485</b>	<b>273</b>	<b>332</b>	796	854	<b>604</b>	<b>598</b>	<b>318</b>	<b>352</b>
MSG-V	<b>524</b>	<b>575</b>	639	720	<b>194</b>	<b>236</b>	<b>536</b>	<b>643</b>	670	702	<b>211</b>	<b>268</b>	<u>603</u>	737	520	<u>564</u>	368	473	<u>778</u>	842	800	890	348	427

Table 2: Quantitative evaluation on ICL-NUIM and Middlebury datasets. All metrics are in thousandths. Lower values correspond to better results, the best result is in bold, the second best is underlined.

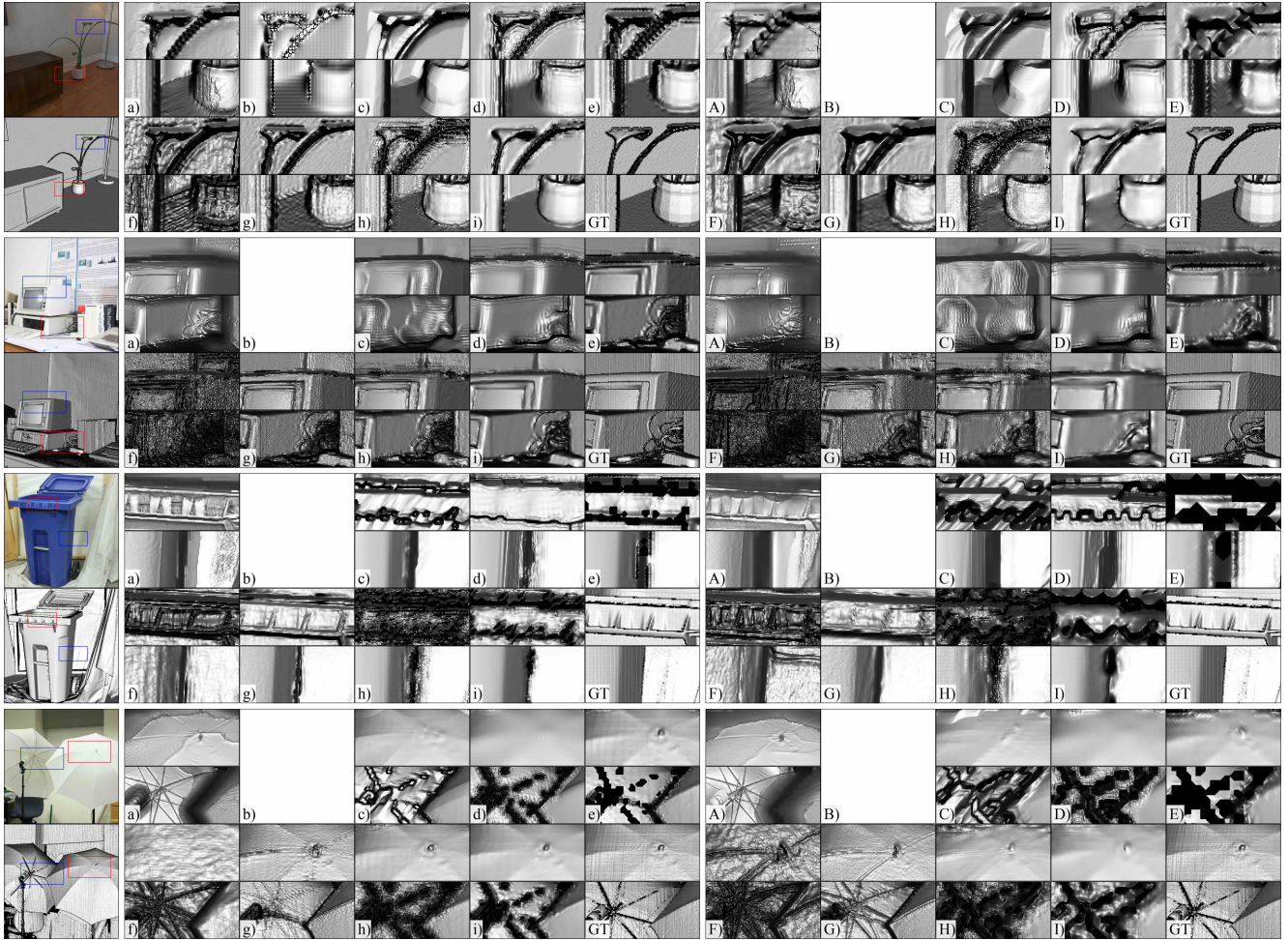


Figure 6: Depth map renderings corresponding to super-resolution results on "Plant" from ICL-NUIM and "Vintage", "Recycle" and "Umbrella" from Middlebury datasets. The left half of the images with lowercase labels correspond to the scaling factor of 4, and the right half with uppercase labels correspond to the scaling factor of 8. a) SRfS [14], b) EG [54], c) PDN [39], d) DG [13], e) Bicubic, f) DIP [47], g) DIP-V, h) MSG [22], i) MSG-V. The method b) failed completely on the Middlebury dataset. Best viewed in zoom.

## References

- [1] G. Agresti, L. Minto, G. Marin, and P. Zanuttigh. Deep learning for confidence information in stereo and tof data fusion. In *Proceedings of the IEEE Conference on Computer Vision and Pattern Recognition*, pages 697–705, 2017. 3
- [2] P. Bojanowski, A. Joulin, D. Lopez-Pas, and A. Szlam. Optimizing the latent space of generative networks. In J. Dy and A. Krause, editors, *Proceedings of the 35th International Conference on Machine Learning*, volume 80 of *Proceedings of Machine Learning Research*, pages 600–609, Stockholmssan, Stockholm Sweden, 10–15 Jul 2018. PMLR. 5
- [3] D. J. Butler, J. Wulff, G. B. Stanley, and M. J. Black. A naturalistic open source movie for optical flow evaluation. In A. Fitzgibbon et al. (Eds.), editor, *European Conf. on Computer Vision (ECCV)*, Part IV, LNCS 7577, pages 611–625. Springer-Verlag, Oct. 2012. 6
- [4] B. Chen and C. Jung. Single depth image super-resolution using convolutional neural networks. In *2018 IEEE International Conference on Acoustics, Speech and Signal Processing (ICASSP)*, pages 1473–1477. IEEE, 2018. 3
- [5] Z. Chen, V. Badrinarayanan, G. Drozdov, and A. Rabinovich. Estimating depth from rgb and sparse sensing. *CoRR*, abs/1804.02771, 2018. 2
- [6] X. Cheng, P. Wang, and R. Yang. Depth estimation via affinity learned with convolutional spatial propagation network. In *European Conference on Computer Vision*, pages 108–125. Springer, Cham, 2018. 2
- [7] M. Cheon, J.-H. Kim, J.-H. Choi, and J.-S. Lee. Generative adversarial network-based image super-resolution using perceptual content losses. In L. Leal-Taixé and S. Roth, editors, *ECCV Workshops*, pages 51–62, Cham, 2019. Springer International Publishing. 3
- [8] N. Chodosh, C. Wang, and S. Lucey. Deep convolutional compressed sensing for lidar depth completion. *arXiv preprint arXiv:1803.08949*, 2018. 2
- [9] D. Eigen, C. Puhrsch, and R. Fergus. Depth map prediction from a single image using a multi-scale deep network. In *Advances in neural information processing systems*, pages 2366–2374, 2014. 2
- [10] D. Ferstl, C. Reinbacher, R. Ranftl, M. R  ther, and H. Bischof. Image guided depth upsampling using anisotropic total generalized variation. In *Proceedings of the IEEE International Conference on Computer Vision*, pages 993–1000, 2013. 5
- [11] D. Ferstl, M. R  ther, and H. Bischof. Variational depth superresolution using example-based edge representations. In *Proceedings of the IEEE International Conference on Computer Vision*, pages 513–521, 2015. 3
- [12] M. W. Gondal, B. Sch  lkopf, and M. Hirsch. The unreasonable effectiveness of texture transfer for single image super-resolution. In *ECCV*, pages 80–97. Springer, 2018. 3
- [13] S. Gu, W. Zuo, S. Guo, Y. Chen, C. Chen, and L. Zhang. Learning dynamic guidance for depth image enhancement. In *Proceedings of the IEEE Conference on Computer Vision and Pattern Recognition*, pages 3769–3778, 2017. 3, 4, 5, 7, 9, 15, 22, 23, 24, 25
- [14] B. Haefner, Y. Qu  au, T. M  llenhoff, and D. Cremers. Fight ill-posedness with ill-posedness: Single-shot variational depth super-resolution from shading. In *Proceedings of the IEEE Conference on Computer Vision and Pattern Recognition*, pages 164–174, 2018. 3, 4, 5, 7, 9, 15, 22, 23, 24, 25
- [15] B. Ham, M. Cho, and J. Ponce. Robust guided image filtering using nonconvex potentials. *IEEE transactions on pattern analysis and machine intelligence*, 40(1):192–207, 2018. 3
- [16] W. Han, S. Chang, D. Liu, M. Yu, M. Witbrock, and T. S. Huang. Image super-resolution via dual-state recurrent networks. In *Proc. CVPR*, 2018. 3
- [17] A. Handa, T. Whelan, J. McDonald, and A. Davison. A benchmark for RGB-D visual odometry, 3D reconstruction and SLAM. In *IEEE Intl. Conf. on Robotics and Automation, ICRA*, Hong Kong, China, May 2014. 5
- [18] M. Haris, G. Shakhnarovich, and N. Ukita. Deep back-projection networks for super-resolution. In *Proc. CVPR*, 2018. 3
- [19] K. Honauer, O. Johannsen, D. Kondermann, and B. Goldluecke. A dataset and evaluation methodology for depth estimation on 4d light fields. In *Asian Conference on Computer Vision*, pages 19–34. Springer, 2016. 2, 12
- [20] K. Honauer, L. Maier-Hein, and D. Kondermann. The hci stereo metrics: Geometry-aware performance analysis of stereo algorithms. In *Proceedings of the IEEE International Conference on Computer Vision*, pages 2120–2128, 2015. 2, 12
- [21] J. Hua and X. Gong. A normalized convolutional neural network for guided sparse depth upsampling. In *IJCAI*, pages 2283–2290, 2018. 2
- [22] T.-W. Hui, C. C. Loy, and X. Tang. Depth map super-resolution by deep multi-scale guidance. In *European Conference on Computer Vision*, pages 353–369. Springer, 2016. 2, 4, 5, 7, 9, 15, 22, 23, 24, 25
- [23] F. N. Iandola, S. Han, M. W. Moskewicz, K. Ashraf, W. J. Dally, and K. Keutzer. Squeezenet: Alexnet-level accuracy with 50x fewer parameters and  0.5mb model size. In *The IEEE Conference on Computer Vision and Pattern Recognition (CVPR)*, 2016. 4
- [24] Z. Jiang, Y. Hou, H. Yue, J. Yang, and C. Hou. Depth super-resolution from rgb-d pairs with transform and spatial domain regularization. *IEEE Transactions on Image Processing*, 27(5):2587–2602, 2018. 3
- [25] J. Johnson, A. Alahi, and L. Fei-Fei. Perceptual losses for real-time style transfer and super-resolution. In *ECCV*, 2016. 3
- [26] B. Kim, J. Ponce, and B. Ham. Deformable Kernel Networks for Joint Image Filtering. working paper or preprint, Oct. 2018. 2
- [27] A. Krizhevsky, I. Sutskever, and G. E. Hinton. Imagenet classification with deep convolutional neural networks. In *Advances in neural information processing systems*, pages 1097–1105, 2012. 4
- [28] C. Ledig, L. Theis, F. Huszar, J. Caballero, A. Cunningham, A. Acosta, A. Aitken, A. Tejani, J. Totz, Z. Wang, and W. Shi. Photo-realistic single image super-resolution using a generative adversarial network. In *Proc. CVPR*, pages 105–114, 2017. 3
- [29] B. Li, Y. Zhou, Y. Zhang, and A. Wang. Depth image super-resolution based on joint sparse coding. *Pattern Recognition Letters*, 2018. 3



- [30] Y. Li, J.-B. Huang, N. Ahuja, and M.-H. Yang. Deep joint image filtering. In *European Conference on Computer Vision*, pages 154–169. Springer, 2016. 2
- [31] X. Luo, R. Chen, Y. Xie, Y. Qu, and C. Li. Bi-gans-st for perceptual image super-resolution. In L. Leal-Taixé and S. Roth, editors, *ECCV Workshops*, pages 20–34, Cham, 2019. Springer International Publishing. 3
- [32] C. Ma, C.-Y. Yang, X. Yang, and M.-H. Yang. Learning a no-reference quality metric for single-image super-resolution. *Computer Vision and Image Understanding*, 158:1 – 16, 2017. 3
- [33] F. Ma, G. V. Cavalheiro, and S. Karaman. Self-supervised sparse-to-dense: Self-supervised depth completion from lidar and monocular camera. *arXiv preprint arXiv:1807.00275*, 2018. 2
- [34] F. Mal and S. Karaman. Sparse-to-dense: Depth prediction from sparse depth samples and a single image. In *2018 IEEE International Conference on Robotics and Automation (ICRA)*, pages 1–8. IEEE, 2018. 2, 4, 5
- [35] R. Mantiuk, K. J. Kim, A. G. Rempel, and W. Heidrich. Hdr-vdp-2: a calibrated visual metric for visibility and quality predictions in all luminance conditions. In *ACM Transactions on graphics (TOG)*, volume 30, page 40. ACM, 2011. 2
- [36] R. Mechrez, I. Talmi, F. Shama, and L. Zelnik-Manor. Learning to maintain natural image statistics. *arXiv preprint arXiv:1803.04626*, 2018. 3
- [37] A. Paszke, S. Gross, S. Chintala, G. Chanan, E. Yang, Z. DeVito, Z. Lin, A. Desmaison, L. Antiga, and A. Lerer. Automatic differentiation in pytorch. In *NIPS-W*, 2017. 6
- [38] S. Peng, B. Haefner, Y. Queau, and D. Cremers. Depth super-resolution meets uncalibrated photometric stereo. In *Proceedings of the IEEE International Conference on Computer Vision*, pages 2961–2968, 2017. 3
- [39] D. Riegler, Gernot aand Ferstl, M. Rüther, and H. Bischof. A deep primal-dual network for guided depth super-resolution. In *British Machine Vision Conference*. The British Machine Vision Association, 2016. 2, 4, 5, 7, 9, 15, 22, 23, 24, 25
- [40] D. Scharstein, H. Hirschmüller, Y. Kitajima, G. Krathwohl, N. Nešić, X. Wang, and P. Westling. High-resolution stereo datasets with subpixel-accurate ground truth. In *German Conference on Pattern Recognition*, pages 31–42. Springer, 2014. 5
- [41] K. Simonyan and A. Zisserman. Very deep convolutional networks for large-scale image recognition. *CoRR*, abs/1409.1556, 2014. 4
- [42] S. Song, S. P. Lichtenberg, and J. Xiao. Sun rgb-d: A rgb-d scene understanding benchmark suite. In *Proceedings of the IEEE conference on computer vision and pattern recognition*, pages 567–576, 2015. 5
- [43] X. Song, Y. Dai, and X. Qin. Deep depth super-resolution: Learning depth super-resolution using deep convolutional neural network. In *Asian Conference on Computer Vision*, pages 360–376. Springer, 2016. 2, 3
- [44] X. Song, Y. Dai, and X. Qin. Deeply supervised depth map super-resolution as novel view synthesis. *IEEE Transactions on Circuits and Systems for Video Technology*, 2018. 3
- [45] A. Tsuchiya, D. Sugimura, and T. Hamamoto. Depth up-sampling by depth prediction. In *2017 IEEE International Conference on Image Processing (ICIP)*, pages 1662–1666, Sept 2017. 3
- [46] J. Uhrig, N. Schneider, L. Schneider, U. Franke, T. Brox, and A. Geiger. Sparsity invariant cnns. In *IEEE International Conference on 3D Vision (3DV)*, 2017. 2
- [47] D. Ulyanov, A. Vedaldi, and V. Lempitsky. Deep image prior. In *The IEEE Conference on Computer Vision and Pattern Recognition (CVPR)*, June 2018. 4, 5, 7, 9, 15, 22, 23, 24, 25
- [48] S. Van der Walt, J. L. Schönberger, J. Nunez-Iglesias, F. Boulogne, J. D. Warner, N. Yager, E. Gouillart, and T. Yu. scikit-image: image processing in python. *PeerJ*, 2:e453, 2014. 12
- [49] T. Vu, T. M. Luu, and C. D. Yoo. Perception-enhanced image super-resolution via relativistic generative adversarial networks. In L. Leal-Taixé and S. Roth, editors, *ECCV 2018 Workshops*, pages 98–113, Cham, 2019. Springer International Publishing. 3
- [50] X. Wang, K. Yu, C. Dong, and C. C. Loy. Recovering realistic texture in image super-resolution by deep spatial feature transform. In *Proc. CVPR*, June 2018. 3
- [51] Z. Wang, A. C. Bovik, H. R. Sheikh, and E. P. Simoncelli. Image quality assessment: from error visibility to structural similarity. *IEEE transactions on image processing*, 13(4):600–612, 2004. 2, 4
- [52] Z. Wang, E. P. Simoncelli, and A. C. Bovik. Multiscale structural similarity for image quality assessment. In *The Thirty-Seventh Asilomar Conference on Signals, Systems & Computers*, 2003, volume 2, pages 1398–1402. IEEE, 2003. 2
- [53] Y. Xiao, X. Cao, X. Zhu, R. Yang, and Y. Zheng. Joint convolutional neural pyramid for depth map super-resolution. *arXiv preprint arXiv:1801.00968*, 2018. 2
- [54] J. Xie, R. S. Feris, and M.-T. Sun. Edge-guided single depth image super resolution. *IEEE Transactions on Image Processing*, 25(1):428–438, 2016. 4, 5, 7, 9, 15, 22, 23, 24
- [55] S. Yan, C. Wu, L. Wang, F. Xu, L. An, K. Guo, and Y. Liu. Ddrnet: Depth map denoising and refinement for consumer depth cameras using cascaded cnns. In *Proceedings of the European Conference on Computer Vision (ECCV)*, pages 151–167, 2018. 2, 4, 5
- [56] J. Yang, X. Ye, K. Li, C. Hou, and Y. Wang. Color-guided depth recovery from rgb-d data using an adaptive autoregressive model. *IEEE transactions on image processing*, 23(8):3443–3458, 2014. 3
- [57] W. Yifan, F. Perazzi, B. McWilliams, A. Sorkine-Hornung, O. Sorkine-Hornung, and C. Schroers. A fully progressive approach to single-image super-resolution. In *CVPR Workshops*, June 2018. 3
- [58] L. Zhang, L. Zhang, X. Mou, D. Zhang, et al. Fsim: a feature similarity index for image quality assessment. *IEEE transactions on Image Processing*, 20(8):2378–2386, 2011. 2
- [59] R. Zhang, P. Isola, A. A. Efros, E. Shechtman, and O. Wang. The unreasonable effectiveness of deep features as a perceptual metric. In *The IEEE Conference on Computer Vision and Pattern Recognition (CVPR)*, June 2018. 2, 4, 6, 12
- [60] Y. Zhang, K. Li, K. Li, L. Wang, B. Zhong, and Y. Fu. Image super-resolution using very deep residual channel attention networks. In *ECCV*, 2018. 3
- [61] Y. Zhang, Y. Tian, Y. Kong, B. Zhong, and Y. Fu. Residual dense network for image super-resolution. In *Proc. CVPR*, June 2018. 3

- [62] H. Zhao, O. Gallo, I. Frosio, and J. Kautz. Loss functions for image restoration with neural networks. *IEEE Transactions on Computational Imaging*, 3(1):47–57, 2017. 3
- [63] L. Zhao, H. Bai, J. Liang, B. Zeng, A. Wang, and Y. Zhao. Simultaneously color-depth super-resolution with conditional generative adversarial network. *arXiv preprint arXiv:1708.09105*, 2017. 3
- [64] Y. Zuo, Q. Wu, J. Zhang, and P. An. Minimum spanning forest with embedded edge inconsistency measurement model for guided depth map enhancement. *IEEE Transactions on Image Processing*, 27(8):4145–4159, 2018. 3

## Supplementary material

### A. Additional evaluation details

In the literature on range-image processing, the term *depth* denotes three different types of range data:

- *disparity* (e.g., Middlebury 2014 dataset), commonly denoting the difference in image location of a feature within two stereo images;
- *orthogonal depth* (e.g., ICL-NUIM and SUN-RGBD datasets and the high resolution scans in the ToFMark dataset), corresponding to the distance from a point in the 3D-space to the image plane;
- *perspective depth* (e.g., low-resolution scans in the ToFMark dataset), corresponding to the distance from a point in the 3D-space to the camera.

We do not generally differentiate between these three types of range data and use the term *depth map* to denote any data of this kind. However, in our experiments we use the exact type of depth that a method was designed for. For evaluation of the methods designed for disparity processing, we calculate virtual disparity images with the baseline of 20 cm for the datasets, containing either orthogonal or perspective depth.

Here we describe the metrics that we consider in addition to the metrics discussed in the main text. We denote the metrics that compare two depth maps  $d_1$  and  $d_2$  with underscore “d”, and the metrics that compare the two corresponding renderings  $I_1$  and  $I_2$  with underscore “v”. We denote the value of, e.g.,  $d_1$  in the pixel with indices  $(i, j)$  by  $d_{1,ij}$  and the total number of pixels by  $N$ . For rendering we calculate the intensity values in the  $[0, 1]$  range.

*BadPix* measures the fraction of the pixels with deviation larger than a certain threshold. We denote the version of this metric that measures absolute deviation with threshold  $\tau$  by  $\text{BadPix}(\tau)$ , and the version that measures *relative* deviation with threshold corresponding to  $\tau$  percents by  $\text{BadPix}(\tau\%)$ . They are calculated as

$$\text{BadPix}_d(\tau|d_1, d_2) = \frac{1}{N} |\{ij : |d_{1,ij} - d_{2,ij}| > \tau\}|,$$

$$\text{BadPix}_d(\tau\%|d_1, d_2) = \frac{1}{N} |\{ij : |\frac{d_{1,ij} - d_{2,ij}}{d_{2,ij}}| > \frac{\tau}{100}\}|,$$

for depth maps and in the same way for renderings. For depth map comparison we consider absolute thresholds of 1 cm, 5 cm and 10 cm and relative thresholds of 1%, 5% and 10%. For renderings we consider the absolute thresholds of 1, 5 and 10 divided by 255, which correspond to deviations by the respective numbers of shades of gray in 8-bit grayscale images.

*Bumpiness*, introduced in [20] for piece-wise planar regions as a measure of nonplanarity, was generalized in [19] to arbitrary depth maps. It is calculated as

$$\text{Bumpiness}_d(d_1, d_2) = \frac{1}{N} \sum_{ij} \min(0.05, \|H_{d_1-d_2}(i, j)\|_F) \cdot 100,$$

where  $\|\cdot\|_F$  denotes Frobenius norm and  $H_f(i, j)$  is the Hessian matrix of the function  $f$ , calculated at point  $(i, j)$ . For calculation of this metric we use the implementation of [19]<sup>3</sup>. Since this metric was originally applied to disparity maps, for its calculation we convert the depth maps to disparity using the camera intrinsics corresponding to the evaluation dataset from [19].

We use the implementation of DSSIM from *scikit-image* [48]<sup>4</sup> and the original implementation of LPIPS from [59]<sup>5</sup>. For calculation of our  $\text{RMSE}_v$  and rendering we calculate the normals using first-order finite-differences.

In addition to our  $\text{RMSE}_v$  we calculate RMS difference of two rendered images without averaging over the basis renderings. We denote this metric as  $\text{RMSE}_v^1$ : for a certain light direction  $e$  it is calculated as

$$\text{RMSE}_v^1(d_1, d_2) = \sqrt{\frac{1}{N} \sum_{i,j} \|e \cdot n_{1,ij} - e \cdot n_{2,ij}\|_2^2}.$$

### B. Evaluation of metrics

In Figures 10-15 we compare the relations between different quality measures. For different subsets of the metrics we explore pair-wise correlations between metric pairs from this subset using scatter plots in the lower half of the figure and Pearson and Spearman correlation coefficients in the upper half of the figure. For reference, on the diagonal of the figure we also include kernel density estimates of metric value distributions for each super-resolution method. The distributions for the modified methods DIP-v and MSG-v are represented with the dashed black and solid black curves respectively.

For the samples from Middlebury and SUN RGB-D datasets, the methods, that do not perform prior inpainting step (including MSG-v), sometimes produce severe outliers in the regions around missing measurements. To minimize

<sup>3</sup>[github.com/lightfield-analysis/evaluation-toolkit](https://github.com/lightfield-analysis/evaluation-toolkit)

<sup>4</sup>[scikit-image.org](https://scikit-image.org)

<sup>5</sup>[github.com/richzhang/PerceptualSimilarity](https://github.com/richzhang/PerceptualSimilarity)

the influence of these outliers on the results of the metric comparison, we limit the  $\text{RMSE}_d$  value to a maximum of 0.5 meters. Among the collected super-resolved images, 8% exceed this threshold.

For each metric, applied to rendered images, we gather the values of this metric for four different light directions and two additional values corresponding to the worst of the first four and their average. We denote the respective versions of the metric with suffixes  $e_1, e_2, e_3, e_4, \text{max}$  and  $\text{avg}$ , where the order of the light directions corresponds to the order in Figure 2. We find that these versions of each metric are strongly correlated (see Figures 10-12), so we further focus on the "worst" version.

In Figure 10 we also compare different versions of  $\text{RMSE}_v^1$  with our  $\text{RMSE}_v$  and find that all the metrics produce very close results. It is consistent with the observation that if  $\text{RMSE}_v$  is bounded by a constant  $C$ , then for *any* choice of  $e$ ,  $\text{RMSE}_v^1$  is bounded by  $C$ , which can be easily seen from the fact that  $\text{RMSE}_v$  does not depend on the choice of an orthonormal basis, so we can choose one of the basis light directions to be equal to  $e$ .

In Figure 13 we compare the metrics of different types: pixel-wise  $\text{RMSE}_d$ ,  $\text{BadPix}_d(5\text{cm})$  and  $\text{BadPix}_d(5\%)$  applied to depth directly; "worst" versions of pixel-wise  $\text{BadPix}_v(5)$  and perceptual  $\text{DSSIM}_v$  and  $\text{LPIPS}_v$ , applied to rendered images; geometrical  $\text{Bumpiness}_d$  and our  $\text{RMSE}_v$ .

We find that all three pixel-wise metrics applied to depth directly demonstrate weak correlation with visual and geometrical metrics. Pixel-wise  $\text{BadPix}_v(5)$  applied to rendered images, although strongly correlated with perceptual metrics, is inappropriate for gradient-based optimization. Additional comparison of pixel-wise  $\text{BadPix}_d$  and  $\text{BadPix}_v$  with different thresholds to perceptual  $\text{DSSIM}_v$  and  $\text{LPIPS}_v$  (see Figures 14 and 15) leads to the same conclusions.  $\text{Bumpiness}_d$  is also strongly correlated with perceptual metrics but only measures local curvature deviation, while the visual appearance of 3D surface is determined by its local orientation.

## C. Evaluation of methods

In Tables 4-11 we provide the results of quantitative evaluation of super-resolution methods on the datasets SimGeo, ICL-NUIM and Middlebury for "box" downsampling model and scaling factors of 4 and 8. In Table 3 we provide the average values.  $\text{RMSE}_d$  is in millimeters,  $\text{BadPix}$  is in percents,  $\text{DSSIM}_v$ ,  $\text{LPIPS}_v$  and  $\text{RMSE}_v$  are in thousandths. For all visual metrics except  $\text{RMSE}_v$  the given result corresponds to the "worst" version. For all metrics the lower value corresponds to the better result. The best results are highlighted in bold and the second best results are underlined.

In addition to metric values, the last three columns of the tables contain the results of the informal perceptual study collected over approximately 250 subjects. In this study,

for each scene from SimGeo, ICL-NUIM and Middlebury datasets a subject was shown the renderings of super-resolved depth maps, shuffled randomly, and was asked to choose the renderings, the most and second most similar to ground truth. The renderings calculated with the fourth light direction were used. In the row corresponding to a certain method, the values in the columns *User, 1st, User, 2nd* and *Top 2* represent the fractions of the subjects (in percents) who chose the rendering of the super-resolved depth map, produced by this method, as the most similar, second most similar or one of the two most similar to the ground truth respectively. We find that  $\text{RMSE}_v$  is mostly consistent with human judgements.

## D. SUN RGB-D and ToFMark

SimGeo, ICL-NUIM and Middlebury datasets have been our primary evaluation sets, yielding the most pronounced outcomes; however, these datasets contain only noise-free scenes. As we are interested in evaluation of our approach on a diverse set of RGB-D images, we conduct additional experiments using twelve scenes from SUN RGB-D dataset and three scenes from ToFMark dataset that feature real-world noise patterns. However, we observe that increased levels of noise are extremely harmful to all the methods, including those modified with our loss, as they fail to produce reasonable *super-resolution* results (see Figures 7-9). Nevertheless, we include these results into the list of images used to compare the metrics, since such comparison does not imply that one of the images is a valid super-resolution result of a low-resolution version of another.

## E. Training with $\text{MSE}_v$

Since optimization of  $\text{MSE}_v$  alone is ill-posed, for the loss function we use an additional regularization term that penalizes absolute depth deviation. We found that among different regularizers, including  $\text{MSE}_d$ ,  $\text{Lap}_1$  produces the best results. In general, we found that optimization leads to the best results if the terms are weighted in such way that geometrically corresponding depth error and angular normal error result in the same magnitudes of terms. The corresponding value of the weighing parameter  $w$  in Equation (1) is determined by the properties of the training data, such as depth map scaling or field-of-view of the camera.



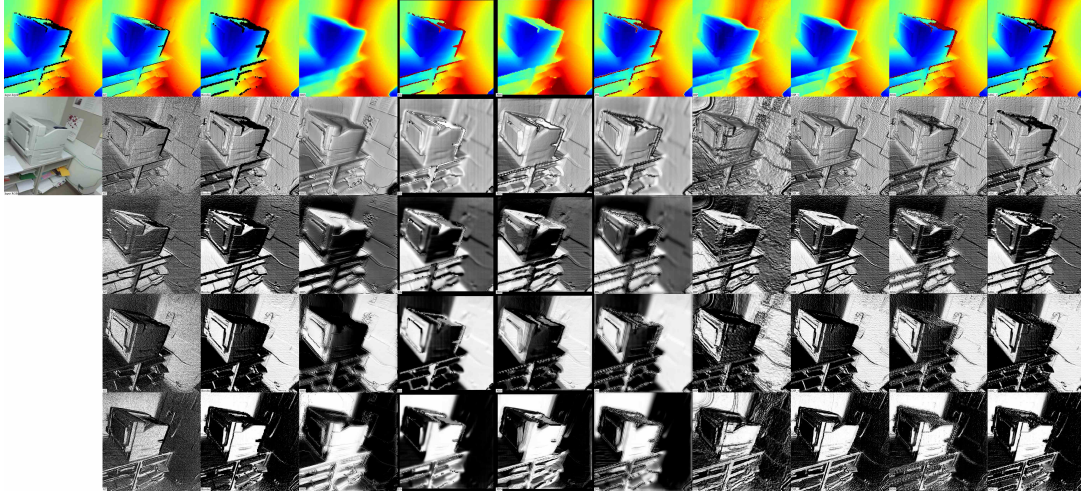


Figure 7: x4 super-resolution results on a Kinect v2 RGB-D scan from SUN RGB-D dataset. Each visualization is labeled in the bottom left corner. Ground truth is in the 2nd column, DIP-v is in the third from the right, MSG-v in the last one.

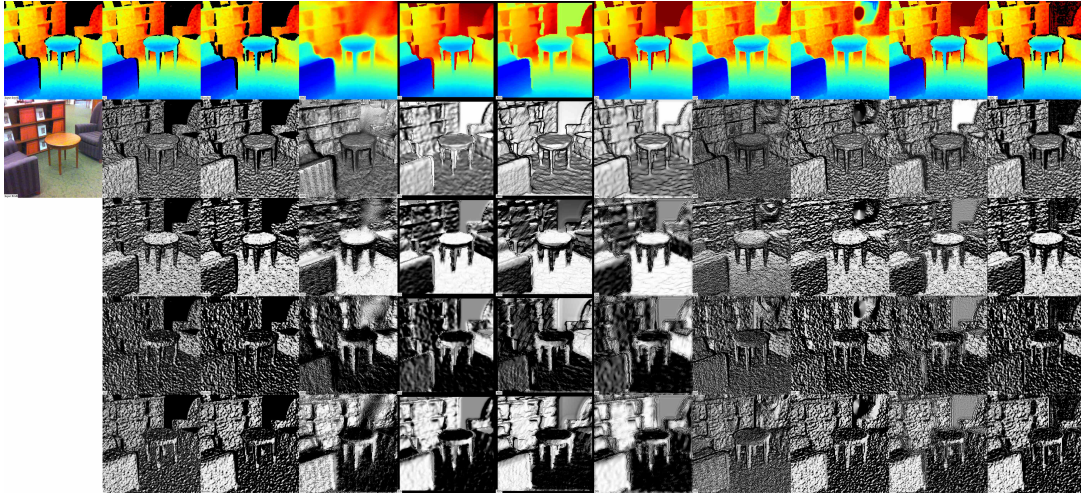


Figure 8: x4 super-resolution results on a RealSense RGB-D scan from SUN RGB-D dataset. Each visualization is labeled in the bottom left corner. Ground truth is in the 2nd column, DIP-v is in the third from the right, MSG-v in the last one.

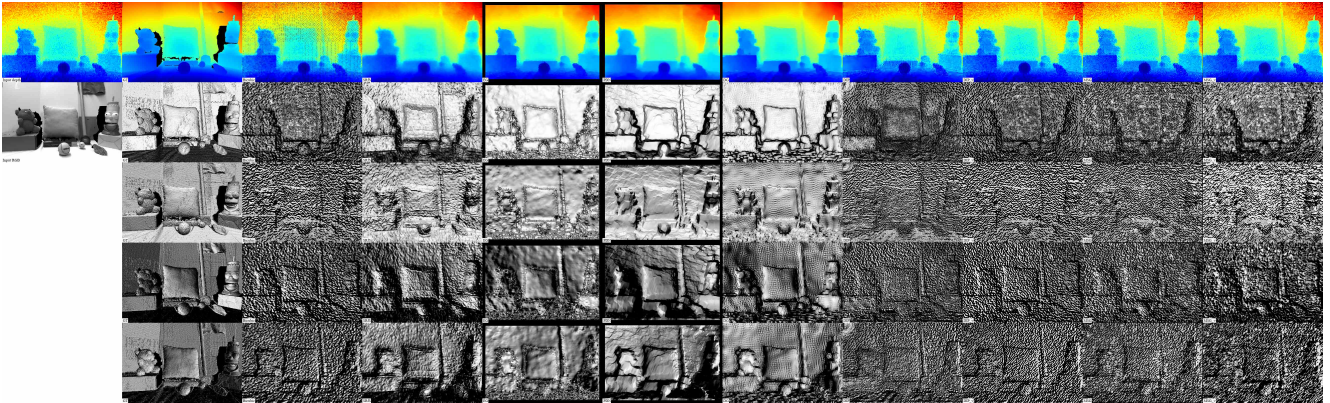


Figure 9: x4 super-resolution results on "Devil" from ToFMark dataset. Each visualization is labeled in the bottom left corner. Ground truth is in the 2nd column, DIP-v is in the third from the right, MSG-v in the last one.

Average performance on SimGeo dataset																	
	RMSE <sub>d</sub>		BadPix <sub>d</sub> (5cm)		BadPix <sub>v</sub> (5)		DSSIM <sub>v</sub>		LPIPS <sub>v</sub>		Bumpiness <sub>d</sub>		RMSE <sub>v</sub>		User, 1st	User, 2nd	Top 2
	x4	x8	x4	x8	x4	x8	x4	x8	x4	x8	x4	x8	x4	x8	x4	x4	x4
Bicubic	55	79	4.1	7.9	23.2	38.3	197	301	320	427	0.70	0.98	193	234	0.5	7.8	8.3
SRfS [14]	61	88	7.5	14.3	74.2	77.1	711	729	869	865	1.48	1.69	311	328	0.0	0.0	0.0
EG [54]	53		2.2		33.1		168		306		0.54		136		0.2	3.9	4.2
PDN [39]	162	211	99.4	99.1	39.2	45.1	224	264	278	407	0.63	0.79	165	201	1.6	12.3	13.8
DG [13]	54	84	3.0	6.4	35.2	39.1	293	316	420	437	0.69	0.82	171	190	0.2	2.9	3.2
DIP [47]	52	59	8.5	12.5	90.5	92.0	887	880	893	915	2.21	2.77	395	475	0.6	0.9	1.5
MSG [22]	39	39	1.5	3.3	51.9	69.3	374	544	569	713	0.79	0.97	194	242	0.4	3.7	4.0
DIP-v	33	41	1.7	2.3	49.7	67.1	313	491	524	598	0.60	0.88	147	174	8.3	59.4	67.8
MSG-v	96	29	0.7	1.5	14.2	34.6	95	206	194	367	0.34	0.46	99	129	88.1	9.1	97.2
Average performance on ICL-NUIM dataset																	
Bicubic	34	54	2.8	5.5	59.3	64.2	431	490	558	668	1.15	1.32	210	252	5.0	28.3	33.3
SRfS [14]	42	62	5.5	11.0	73.5	76.1	641	664	636	660	1.72	1.83	287	314	0.0	0.0	0.0
PDN [39]	135	165	93.8	82.9	66.2	70.2	480	509	623	650	1.14	1.24	237	264	2.6	10.5	13.1
DG [13]	36	58	4.3	6.4	64.4	65.5	497	505	663	689	1.28	1.32	234	259	0.6	5.5	6.1
DIP [47]	43	56	10.6	14.2	83.6	83.4	812	806	690	690	2.73	2.58	394	389	1.1	0.9	2.0
MSG [22]	25	36	1.6	3.5	64.1	69.0	489	557	510	534	1.27	1.46	210	255	1.1	7.2	8.3
DIP-v	28	40	2.6	3.9	67.8	69.6	516	548	407	503	1.45	1.56	209	236	9.6	31.9	41.4
MSG-v	24	41	1.3	3.1	56.3	61.1	387	437	527	602	0.94	1.06	157	192	79.9	11.8	91.7
Average performance on Middlebury dataset																	
Bicubic	843	1139	10.8	13.9	71.5	76.7	648	748	575	720	0.87	0.76	344	386	4.1	25.3	29.4
SRfS [14]	100	145	21.4	33.6	86.4	89.5	780	810	669	704	1.32	1.28	428	461	0.0	0.0	0.0
PDN [39]	173	225	85.3	76.5	83.4	86.4	744	790	653	711	1.38	1.67	405	467	9.9	28.1	37.9
DG [13]	266	330	15.0	24.5	81.8	84.1	765	784	728	740	1.54	1.73	421	442	0.7	10.6	11.3
DIP [47]	72	104	19.6	24.4	92.4	93.4	927	947	737	717	2.82	2.90	565	592	1.2	5.6	6.8
MSG [22]	228	426	10.8	13.1	81.8	87.2	774	858	649	696	1.96	2.19	477	525	0.2	1.6	1.8
DIP-v	56	87	6.4	10.6	83.1	87.4	728	821	506	568	1.34	1.56	353	409	72.3	18.2	90.5
MSG-v	96	133	7.3	9.2	73.3	79.0	667	757	639	690	1.20	1.35	376	431	10.8	9.9	20.7
Average performance on the scenes without missing measurements (SimGeo, ICL-NUIM, Vintage)																	
	RMSE <sub>d</sub>		BadPix <sub>d</sub> (5cm)		BadPix <sub>v</sub> (5)		DSSIM <sub>v</sub>		LPIPS <sub>v</sub>		Bumpiness <sub>d</sub>		RMSE <sub>v</sub>		User, 1st	User, 2nd	Top 2
	x4	x8	x4	x8	x4	x8	x4	x8	x4	x8	x4	x8	x4	x8	x4	x4	x4
Bicubic	46	69	3.5	6.9	43.7	53.3	333	415	452	561	0.97	1.19	206	248	3.0	18.9	21.9
SRfS [14]	55	81	7.3	14.1	74.6	77.4	680	701	743	753	1.60	1.75	303	326	0.0	0.0	0.0
PDN [39]	148	187	94.4	90.1	55.0	59.8	378	412	482	542	0.93	1.06	210	241	1.9	10.5	12.4
DG [13]	47	73	3.9	6.7	52.1	54.4	416	430	561	584	1.02	1.10	209	230	0.4	4.0	4.4
DIP [47]	50	62	10.7	15.9	87.6	88.2	857	853	801	808	2.59	2.79	414	452	0.8	0.8	1.7
MSG [22]	33	39	1.7	3.6	59.8	70.3	454	569	547	622	1.08	1.26	210	258	0.7	5.8	6.4
DIP-v	31	43	2.2	3.3	60.8	69.9	444	548	474	560	1.09	1.32	191	223	10.2	45.5	55.8
MSG-v	38	38	1.1	2.6	38.0	50.1	264	346	385	501	0.69	0.81	135	169	82.7	10.9	93.6
Average performance on the scenes with missing measurements (Middlebury excluding Vintage)																	
Bicubic	972	1313	11.8	14.7	71.3	76.6	663	765	570	718	0.77	0.61	358	400	3.8	24.7	28.5
SRfS [14]	100	145	22.2	33.8	86.9	89.8	790	820	676	716	1.26	1.21	441	474	0.0	0.0	0.0
PDN [39]	178	234	88.3	76.1	83.5	86.6	757	803	644	713	1.36	1.69	419	487	11.5	32.8	44.3
DG [13]	298	367	16.3	26.9	82.2	84.7	781	803	716	724	1.55	1.76	442	465	0.9	12.2	13.1
DIP [47]	72	102	18.8	20.7	92.2	93.3	923	943	708	691	2.62	2.68	549	577	1.2	6.4	7.7
MSG [22]	259	488	12.1	14.1	82.0	87.7	785	870	673	711	2.02	2.24	507	552	0.2	0.2	0.5
DIP-v	58	91	7.1	11.4	82.7	87.2	716	811	494	550	1.23	1.41	354	405	80.1	13.8	93.9
MSG-v	107	145	8.1	9.8	73.6	79.2	688	776	634	688	1.19	1.34	404	458	1.3	8.8	10.1
Average performance on SimGeo, ICL-NUIM, Middlebury																	
Bicubic	339	462	6.1	9.3	52.4	60.6	437	525	489	611	0.91	1.00	254	296	3.3	20.7	24.0
SRfS [14]	69	101	12.0	20.3	78.5	81.3	715	738	722	741	1.50	1.58	347	372	0.0	0.0	0.0
PDN [39]	157	202	92.4	85.7	64.0	68.2	498	536	533	596	1.07	1.26	276	319	5.0	17.5	22.5
DG [13]	126	166	7.8	13.1	61.6	64.0	531	548	610	628	1.19	1.31	283	305	0.5	6.6	7.1
DIP [47]	57	75	13.3	17.4	89.1	89.8	878	881	771	771	2.60	2.76	457	491	1.0	2.6	3.6
MSG [22]	104	181	5.0	6.9	66.8	75.8	559	664	587	650	1.37	1.57	304	350	0.5	4.0	4.6
DIP-v	40	58	3.8	5.9	67.7	75.4	530	631	481	557	1.14	1.34	242	280	32.3	35.5	67.8
MSG-v	60	72	3.3	4.8	49.2	59.3	398	482	464	560	0.85	0.98	220	260	57.0	10.2	67.3

Table 3: Quantitative evaluation summary. The best result is in bold, the second best in underlined.



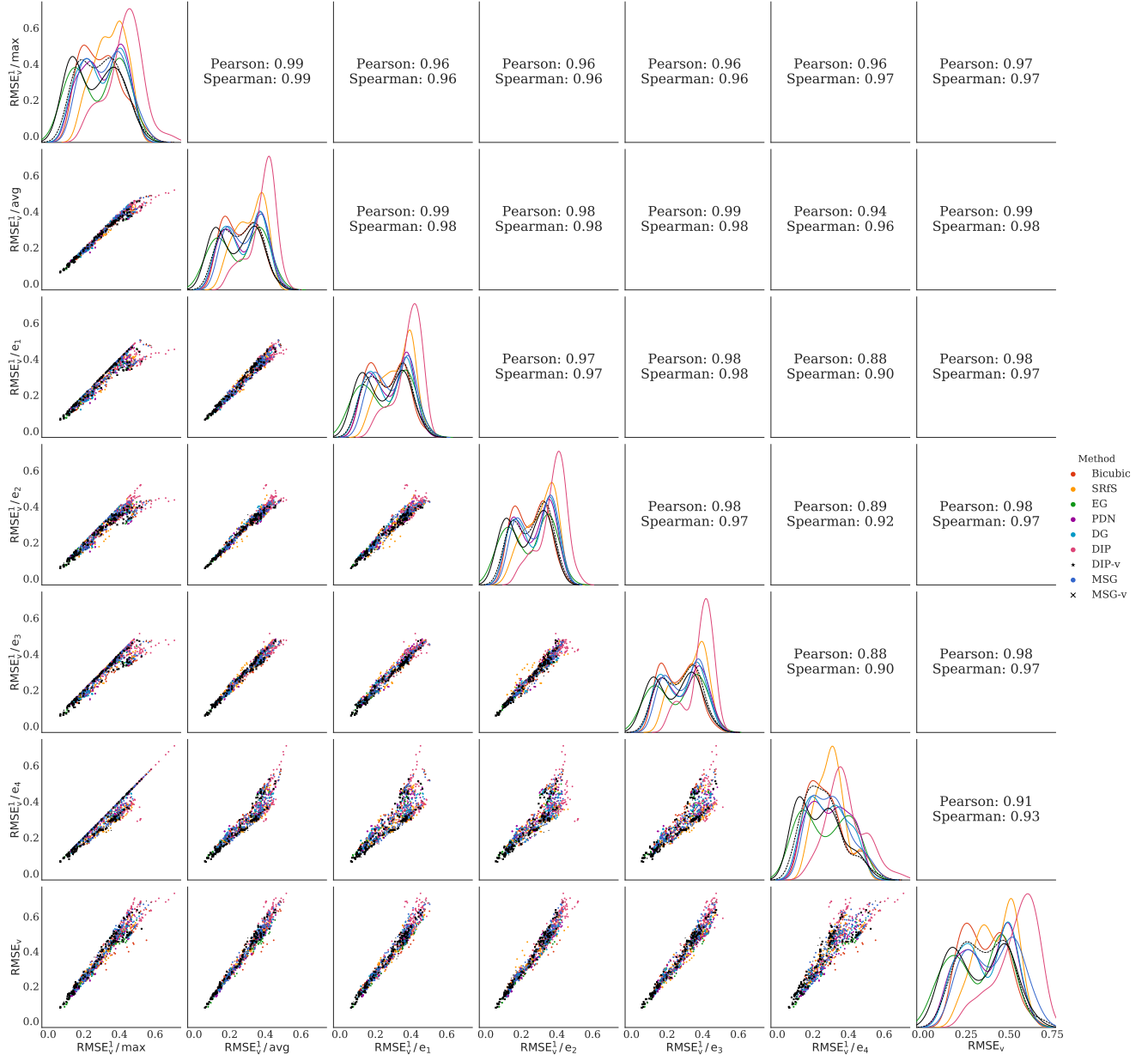


Figure 10: Comparison of different versions of  $RMSE_V^1$  metric and  $RMSE_V$  metric. Best viewed in zoom and color.



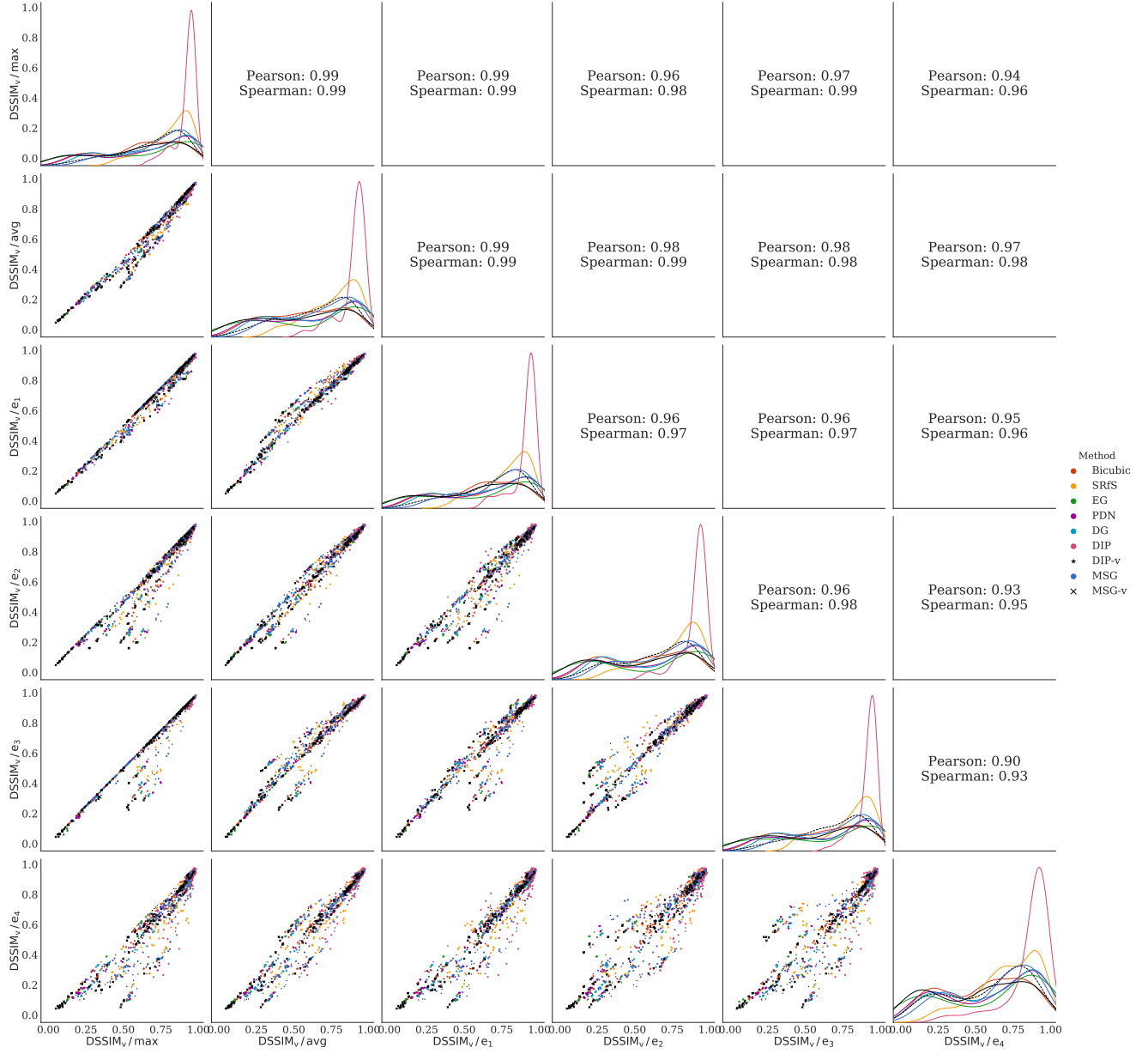


Figure 11: Comparison of different versions of DSSIM<sub>v</sub> metric. Best viewed in zoom and color.

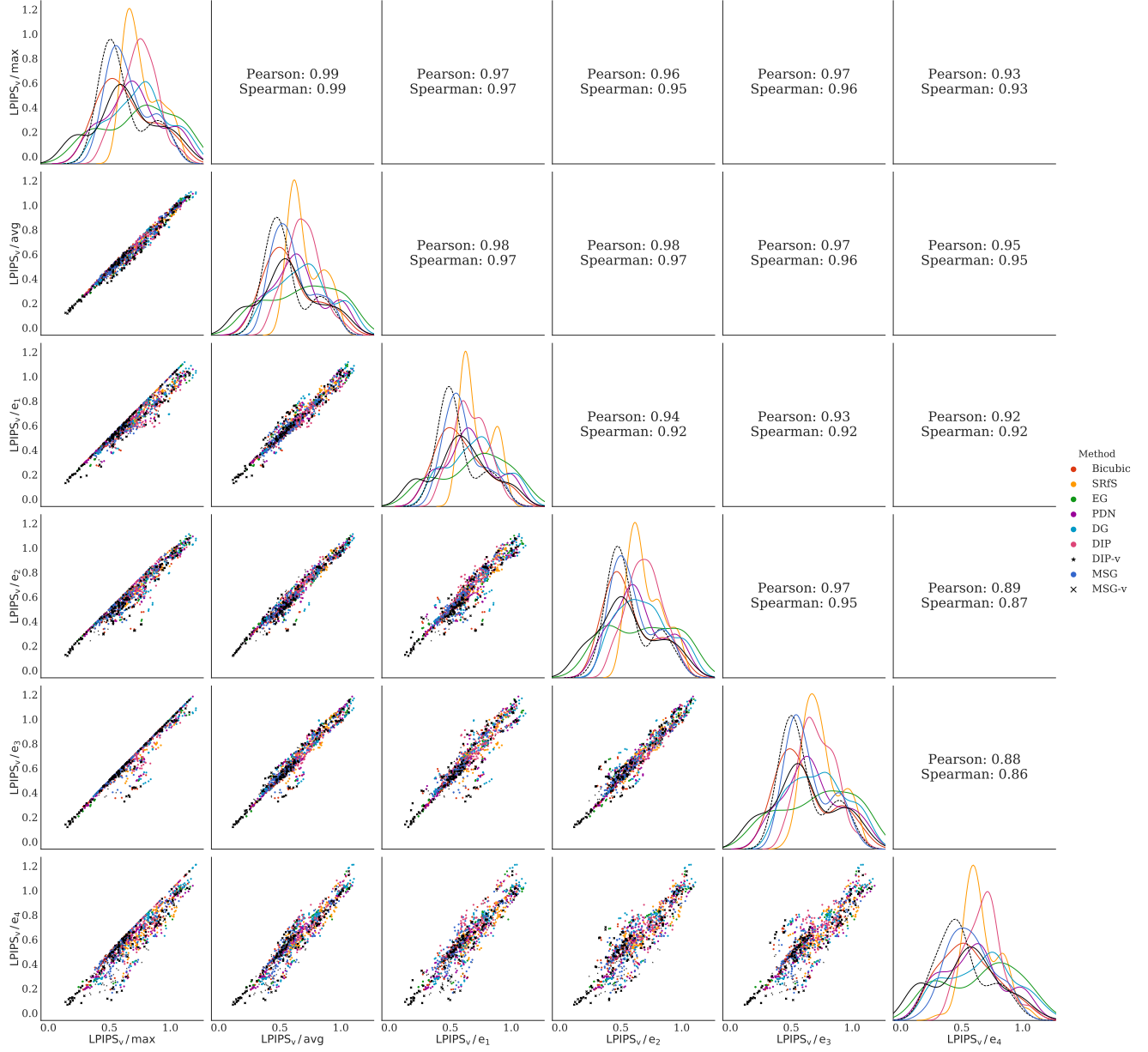


Figure 12: Comparison of different versions of LPIPS<sub>v</sub> metric. Best viewed in zoom and color.

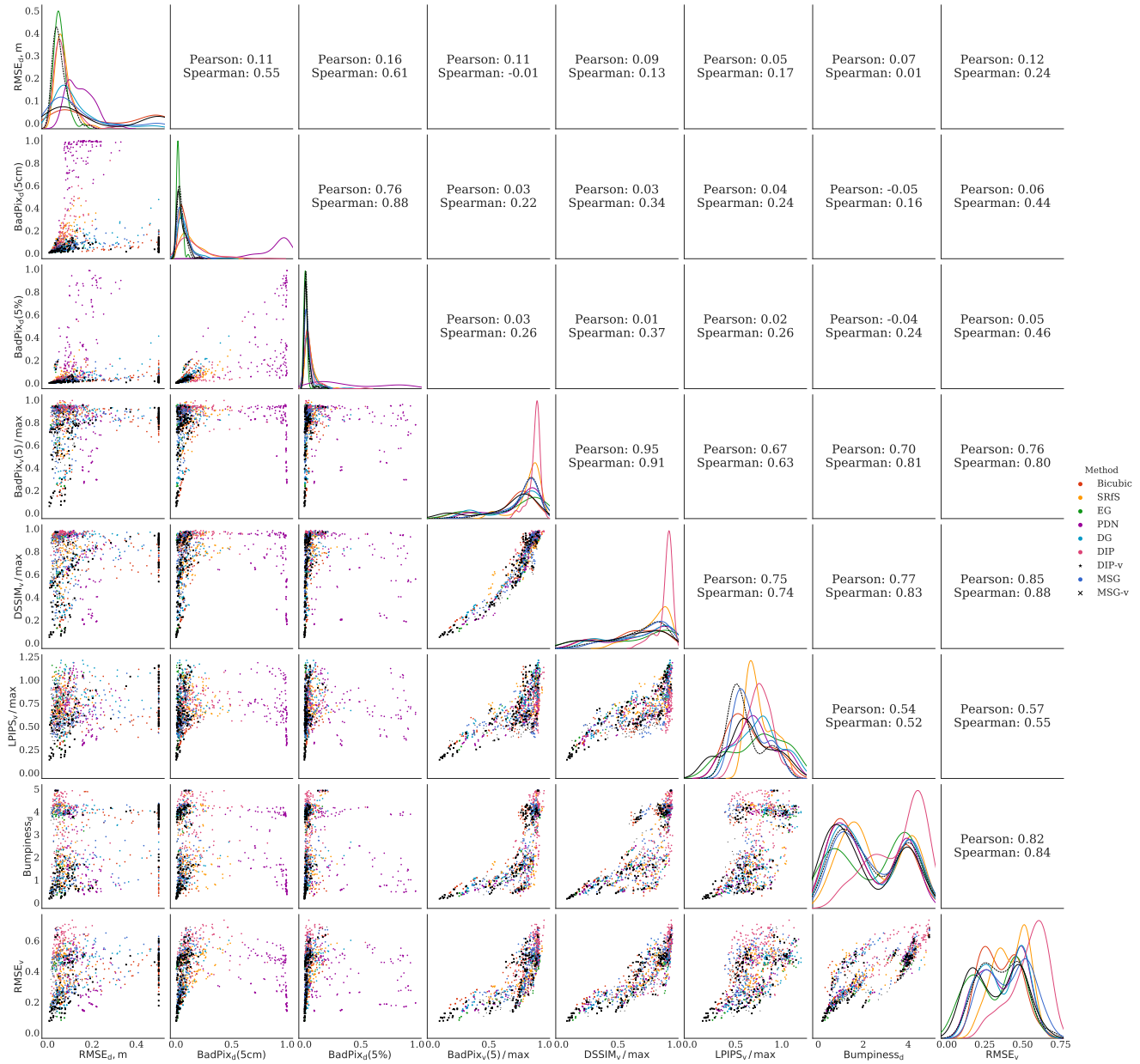


Figure 13: Comparison of metrics of different types. Best viewed in zoom and color.



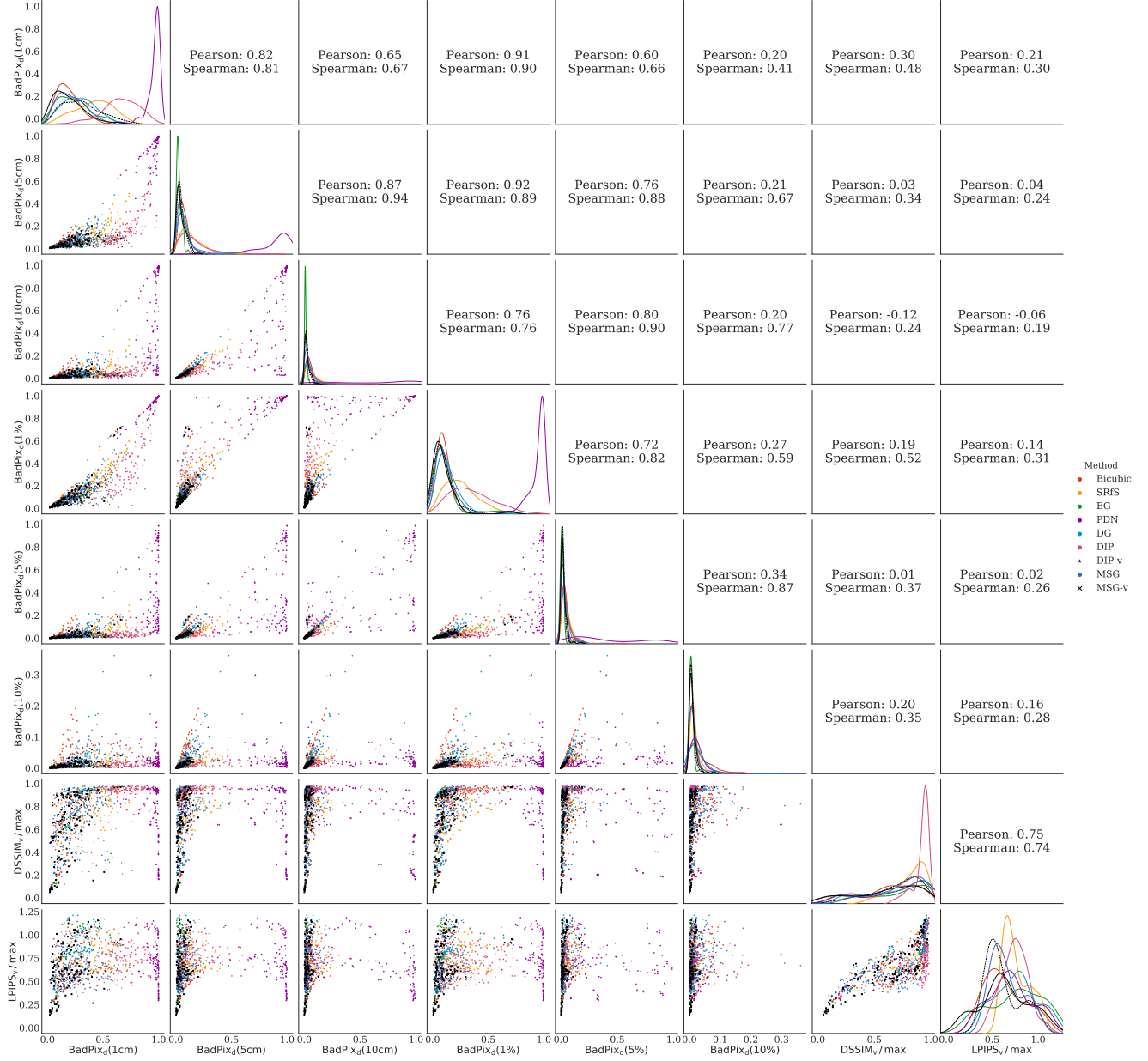


Figure 14: Comparison of different pixel-wise metrics applied to depth directly and perceptual metrics. Best viewed in zoom and color.

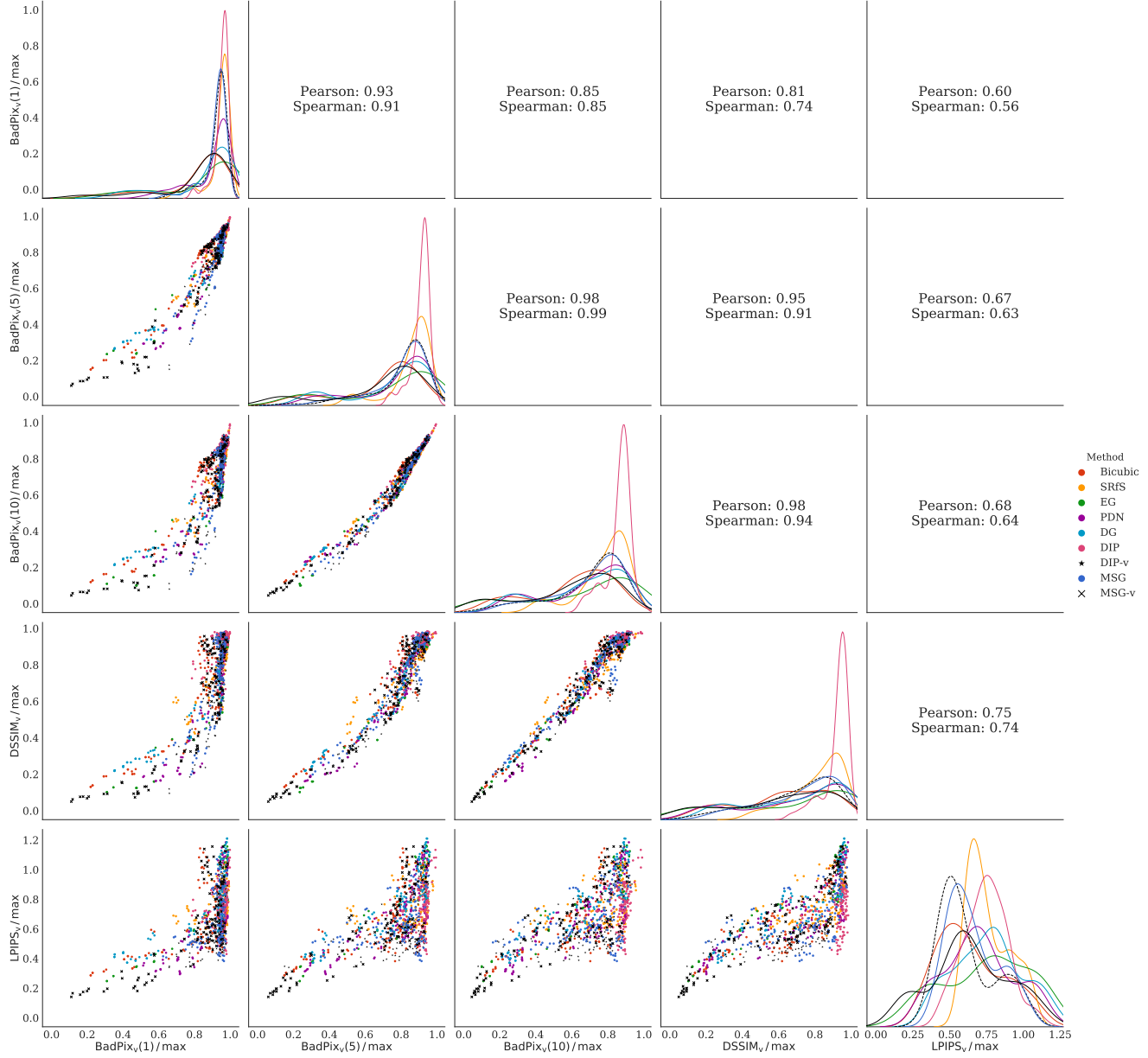


Figure 15: Comparison of different pixel-wise metrics applied to rendered images and perceptual metrics. Best viewed in zoom and color.

Cube, high-frequency texture																	
	RMSE <sub>d</sub>		BadPix <sub>d</sub> (5cm)		BadPix <sub>v</sub> (5)		DSSIM <sub>v</sub>		LPIPS <sub>v</sub>		Bumpiness <sub>d</sub>		RMSE <sub>v</sub>		User, 1st	User, 2nd	Top 2
	x4	x8	x4	x8	x4	x8	x4	x8	x4	x8	x4	x8	x4	x8	x4	x4	x4
Bicubic	44	63	2.7	5.2	<u>15.0</u>	<b>27.3</b>	131	204	287	<u>395</u>	0.43	0.61	160	188	0.7	<u>13.2</u>	14.0
SRfS [14]	52	75	6.2	12.1	89.2	80.3	934	818	1036	938	1.73	1.67	361	339	0.0	0.0	0.0
EG [54]	43		1.2		25.4		<u>113</u>		<u>214</u>		<u>0.35</u>		<u>105</u>		0.7	9.6	10.3
PDN [39]	164	219	99.6	99.4	27.5	<u>29.5</u>	156	<b>186</b>	250	<b>368</b>	0.39	<u>0.49</u>	145	171	0.7	4.4	5.1
DG [13]	44	67	1.9	4.2	26.4	30.1	218	240	411	437	0.44	0.55	139	<u>159</u>	0.7	7.4	8.1
DIP [47]	45	48	6.4	8.5	93.5	92.5	963	947	906	918	2.98	2.50	530	494	0.0	0.7	0.7
MSG [22]	<u>29</u>	38	1.0	2.6	60.1	77.9	445	653	687	877	0.79	0.98	176	233	0.0	0.0	0.0
DIP-v	<b>26</b>	<u>36</u>	<u>0.8</u>	<u>1.6</u>	56.2	60.8	352	413	613	653	0.64	0.89	146	162	<u>5.9</u>	<b>58.1</b>	<u>64.0</u>
MSG-v	102	<b>20</b>	<b>0.3</b>	<b>0.7</b>	<b>9.3</b>	51.0	<b>70</b>	316	<b>179</b>	676	<b>0.20</b>	<b>0.39</b>	<b>77</b>	<b>125</b>	<b>91.2</b>	6.6	<b>97.8</b>
Cube, no texture																	
Bicubic	44	63	2.7	5.2	<u>15.0</u>	<u>27.3</u>	131	204	287	395	0.43	0.61	160	188	0.0	5.9	5.9
SRfS [14]	43	63	2.1	4.5	53.4	51.7	516	476	754	728	0.67	0.89	219	228	0.0	0.0	0.0
EG [54]	43		1.2		25.4		128		<u>282</u>		0.35		<u>105</u>		0.0	2.9	2.9
PDN [39]	164	219	99.6	99.4	26.3	29.3	162	<u>185</u>	314	<u>353</u>	0.38	0.49	145	171	0.7	4.4	5.1
DG [13]	44	67	1.9	4.2	26.4	30.1	218	240	411	437	0.44	0.55	139	159	0.0	2.2	2.2
DIP [47]	72	56	23.2	17.3	94.3	99.1	912	980	1026	1133	2.05	4.22	434	683	0.0	0.7	0.7
MSG [22]	29	<u>26</u>	1.0	1.7	30.7	49.8	199	314	509	642	0.42	0.47	157	171	0.0	<u>6.6</u>	6.6
DIP-v	<u>26</u>	35	<u>0.8</u>	<u>1.4</u>	15.1	45.4	<u>95</u>	237	347	478	<u>0.28</u>	<u>0.35</u>	111	<u>107</u>	<u>1.5</u>	<b>76.5</b>	<u>77.9</u>
MSG-v	<b>9</b>	<b>19</b>	<b>0.3</b>	<b>0.4</b>	<b>6.0</b>	<b>13.0</b>	<b>50</b>	<b>73</b>	<b>141</b>	<b>213</b>	<b>0.17</b>	<b>0.21</b>	<b>77</b>	<b>82</b>	<b>97.8</b>	0.7	<b>98.5</b>

Table 4: Quantitative evaluation on "Cube" with different RGBs from SimGeo dataset. The best result is in bold, the second best is underlined.

Sphere and cylinder, high-frequency texture																	
	RMSE <sub>d</sub>		BadPix <sub>d</sub> (5cm)		BadPix <sub>v</sub> (5)		DSSIM <sub>v</sub>		LPIPS <sub>v</sub>		Bumpiness <sub>d</sub>		RMSE <sub>v</sub>		User, 1st	User, 2nd	Top 2
	x4	x8	x4	x8	x4	x8	x4	x8	x4	x8	x4	x8	x4	x8	x4	x4	x4
Bicubic	57	82	4.1	8.1	<u>20.1</u>	<u>36.7</u>	189	294	313	<u>420</u>	0.67	0.98	189	234	0.0	0.7	0.7
SRfS [14]	70	102	12.1	24.6	91.9	91.8	887	865	1025	1008	2.43	2.41	417	403	0.0	0.0	0.0
EG [54]	55		2.4		30.4		<u>143</u>		326		<u>0.50</u>		<u>130</u>		0.0	1.5	1.5
PDN [39]	157	197	99.3	98.9	40.7	54.1	198	<b>242</b>	<u>295</u>	461	0.60	<u>0.77</u>	150	187	1.5	9.6	11.0
DG [13]	56	87	3.2	6.3	30.9	<b>35.2</b>	265	285	372	<b>386</b>	0.66	<u>0.77</u>	166	180	0.0	1.5	1.5
DIP [47]	46	69	3.9	27.2	97.0	99.2	965	975	1062	1014	4.01	4.80	548	696	1.5	2.9	4.4
MSG [22]	<u>41</u>	<u>41</u>	1.4	3.6	72.6	85.6	626	820	859	960	0.98	1.43	229	314	0.0	0.0	0.0
DIP-v	<b>28</b>	43	<u>1.2</u>	<u>2.4</u>	69.2	86.0	560	850	766	832	0.56	1.45	142	242	<u>32.4</u>	<b>52.9</b>	<u>85.3</u>
MSG-v	99	<b>37</b>	<b>0.6</b>	<b>2.0</b>	<b>14.3</b>	53.0	<b>94</b>	334	<b>267</b>	583	<b>0.29</b>	<b>0.55</b>	<b>96</b>	<b>164</b>	<b>64.7</b>	<u>30.9</u>	<b>95.6</b>
Sphere and cylinder, no texture																	
Bicubic	57	82	4.1	8.1	<u>20.2</u>	36.8	189	294	325	437	0.67	0.98	190	233	0.0	0.7	0.7
SRfS [14]	59	85	4.6	8.6	51.4	70.8	430	619	657	766	0.77	1.25	193	256	0.0	0.0	0.0
EG [54]	56		2.4		30.9		<u>160</u>		383		0.50		<u>128</u>		0.0	1.5	1.5
PDN [39]	157	197	99.3	98.9	38.0	44.1	202	<u>218</u>	294	<u>386</u>	0.58	0.76	150	186	5.9	<u>17.6</u>	23.5
DG [13]	57	87	3.2	6.4	31.0	<u>35.3</u>	265	284	396	409	0.66	0.78	165	180	0.7	2.2	2.9
DIP [47]	49	56	5.0	5.5	85.6	81.6	856	662	927	723	1.01	0.96	244	249	1.5	0.0	1.5
MSG [22]	40	<u>37</u>	<u>1.4</u>	3.1	45.6	64.5	288	444	509	610	0.65	0.76	183	218	0.7	0.7	1.5
DIP-v	<u>35</u>	39	<u>1.4</u>	<u>1.8</u>	41.0	72.6	210	523	517	643	<u>0.47</u>	<u>0.70</u>	130	<u>141</u>	<u>9.6</u>	<b>64.7</b>	<u>74.3</u>
MSG-v	<b>14</b>	<b>27</b>	<b>0.7</b>	<b>1.3</b>	<b>8.5</b>	<b>18.0</b>	<b>77</b>	<b>93</b>	<b>174</b>	<b>200</b>	<b>0.27</b>	<b>0.32</b>	<b>96</b>	<b>110</b>	<b>81.6</b>	12.5	<b>94.1</b>
Sphere and cylinder, low-frequency texture																	
Bicubic	57	82	4.1	8.1	<u>20.1</u>	36.7	189	294	313	420	0.67	0.98	189	234	0.0	2.2	2.2
SRfS [14]	62	91	6.8	14.9	<u>74.9</u>	81.0	691	738	961	956	1.38	1.65	311	335	0.0	0.0	0.0
EG [54]	54		2.4		30.4		<u>160</u>		377		<u>0.50</u>		129		<u>0.7</u>	7.4	8.1
PDN [39]	157	197	99.3	98.9	37.9	44.5	202	219	299	397	0.58	0.76	150	186	<u>0.7</u>	<u>36.0</u>	36.8
DG [13]	56	87	3.2	6.3	30.9	<u>35.2</u>	265	285	372	<u>386</u>	0.66	0.77	166	180	0.0	3.7	3.7
DIP [47]	49	52	8.0	4.9	85.5	84.7	796	812	821	924	1.19	1.18	267	250	0.0	0.0	0.0
MSG [22]	41	<u>41</u>	<u>1.3</u>	3.0	39.6	66.2	264	458	493	612	0.64	0.74	181	213	0.0	1.5	1.5
DIP-v	38	42	1.7	<u>2.2</u>	48.0	60.4	238	351	456	516	<u>0.50</u>	<u>0.61</u>	<u>128</u>	<u>152</u>	<u>0.7</u>	<b>47.8</b>	<u>48.5</u>
MSG-v	<b>16</b>	<b>26</b>	<b>0.7</b>	<b>1.2</b>	<b>8.5</b>	<b>17.5</b>	<b>76</b>	<b>92</b>	<b>156</b>	<b>181</b>	<b>0.27</b>	<b>0.31</b>	<b>97</b>	<b>100</b>	<b>97.8</b>	1.5	<b>99.3</b>

Table 5: Quantitative evaluation on "Sphere and cylinder" with different RGBs from SimGeo dataset. The best result is in bold, the second best is underlined.



	Lucy																
	RMSE <sub>d</sub>		BadPix <sub>d</sub> (5cm)		BadPix <sub>v</sub> (5)		DSSIM <sub>v</sub>		LPIPS <sub>v</sub>		Bumpiness <sub>d</sub>		RMSE <sub>v</sub>		User, 1st	User, 2nd	Top 2
	x4	x8	x4	x8	x4	x8	x4	x8	x4	x8	x4	x8	x4	x8	x4		x4
Bicubic	72	103	6.8	13.0	<u>48.8</u>	<u>65.0</u>	<u>355</u>	<u>519</u>	398	497	1.37	1.74	267	328	<u>2.2</u>	<u>24.3</u>	26.5
SRfS [14]	82	113	13.2	20.8	84.6	87.1	811	857	781	792	1.90	2.28	367	407	0.0	0.0	0.0
EG [54]	69		3.5		56.2		357		426		<u>1.05</u>		<u>220</u>		0.0	0.7	0.7
PDN [39]	173	234	99.0	98.8	64.9	68.9	456	535	368	480	1.24	1.47	251	303	0.0	1.5	1.5
DG [13]	69	108	4.9	11.0	65.5	68.6	523	562	558	565	1.28	1.50	249	281	0.0	0.7	0.7
DIP [47]	<u>53</u>	75	4.7	11.4	87.4	95.2	827	908	615	778	2.02	2.93	344	478	0.7	0.7	1.5
MSG [22]	54	53	2.7	5.4	62.9	71.7	444	577	480	578	1.30	1.42	259	306	1.5	13.2	14.7
DIP-v	<b>44</b>	55	4.6	<u>4.4</u>	69.0	77.5	421	574	446	<u>468</u>	1.15	<u>1.27</u>	223	<u>239</u>	0.0	<b>56.6</b>	<u>56.6</u>
MSG-v	74	<b>47</b>	<b>1.6</b>	<b>3.7</b>	<b>38.8</b>	<b>55.0</b>	<b>205</b>	<b>325</b>	<b>251</b>	<b>348</b>	<b>0.82</b>	<b>0.96</b>	<b>156</b>	<b>195</b>	<b>95.6</b>	2.2	<b>97.8</b>

Table 6: Quantitative evaluation on "Lucy" from SimGeo dataset. The best result is in bold, the second best is underlined.

Painting																	
	RMSE <sub>d</sub>		BadPix <sub>d</sub> (5cm)		BadPix <sub>v</sub> (5)		DSSIM <sub>v</sub>		LPIPS <sub>v</sub>		Bumpiness <sub>d</sub>		RMSE <sub>v</sub>		User, 1st	User, 2nd	Top 2
	x4	x8	x4	x8	x4	x8	x4	x8	x4	x8	x4	x8	x4	x8	x4	x4	x4
Bicubic	28	47	2.5	5.6	57.1	64.1	423	514	544	649	0.95	1.15	213	265	4.4	47.8	52.2
SRfS [14]	39	60	6.5	15.9	78.4	81.2	707	722	612	661	1.47	1.55	308	337	0.0	0.0	0.0
EG [54]	36		3.1		61.9		481		720		0.94		231		0.0	3.7	3.7
PDN [39]	151	215	99.3	99.2	65.2	70.2	488	532	669	709	0.89	1.01	237	275	4.4	10.3	14.7
DG [13]	31	49	2.4	5.5	61.9	63.9	503	506	678	700	1.08	1.13	232	272	0.7	3.7	4.4
DIP [47]	30	37	4.0	4.7	80.4	79.5	802	766	630	612	2.18	1.82	362	341	0.0	0.0	0.0
MSG [22]	21	29	1.2	2.2	63.7	67.9	495	570	475	507	0.97	1.12	203	243	2.2	5.1	7.4
DIP-v	22	32	2.3	3.2	70.1	70.3	567	564	386	501	1.07	1.12	210	239	2.9	21.3	24.3
MSG-v	17	34	0.9	1.8	51.4	58.0	354	410	532	607	0.67	0.77	142	170	85.3	8.1	93.4

Sofa																	
Bicubic	38	58	1.8	3.6	75.4	77.0	566	616	704	764	2.12	2.33	212	250	3.7	15.4	19.1
SRfS [14]	39	58	2.0	3.5	82.3	88.1	715	832	631	743	2.97	3.45	310	405	0.0	0.0	0.0
EG [54]	42		2.5		79.0		598		767		2.28		213		0.0	8.8	8.8
PDN [39]	86	91	71.0	70.8	83.3	83.0	641	658	784	763	2.40	2.50	260	264	0.7	3.7	4.4
DG [13]	41	63	3.2	4.4	77.7	77.9	624	632	823	855	2.30	2.33	255	263	0.0	5.1	5.1
DIP [47]	45	57	7.1	12.7	93.1	94.0	928	946	758	738	3.91	3.99	518	560	0.0	0.0	0.0
MSG [22]	27	36	1.2	2.3	80.6	85.7	718	791	606	610	2.71	3.22	254	316	0.0	0.7	0.7
DIP-v	27	43	0.9	2.0	79.1	82.5	645	718	414	585	2.67	3.07	215	266	19.1	47.8	66.9
MSG-v	35	44	0.7	1.6	74.0	75.7	537	585	710	759	1.96	2.10	165	196	76.5	18.4	94.9

Plant																	
Bicubic	38	58	3.7	6.4	75.9	79.9	562	610	688	763	1.58	1.79	249	290	1.5	22.1	23.5
SRfS [14]	46	65	5.8	9.5	82.9	85.0	658	692	632	649	1.96	2.13	280	309	0.0	0.0	0.0
EG [54]	43		4.5		82.2		568		677		1.64		255		0.0	0.7	0.7
PDN [39]	88	89	94.5	37.8	79.5	82.5	574	612	659	699	1.46	1.60	269	305	4.4	7.4	11.8
DG [13]	40	63	3.9	6.7	79.5	81.1	611	622	745	785	1.67	1.70	268	291	2.2	11.0	13.2
DIP [47]	38	47	6.9	6.1	93.9	92.8	919	880	764	723	4.33	3.95	490	437	0.0	0.7	0.7
MSG [22]	31	44	2.3	3.7	78.0	81.8	571	645	582	495	1.62	1.84	234	285	0.0	11.8	11.8
DIP-v	31	40	4.7	4.8	83.5	84.1	694	707	463	555	2.25	2.21	262	276	11.0	33.1	44.1
MSG-v	27	44	1.8	3.9	74.3	77.8	524	575	639	720	1.31	1.47	194	236	80.9	13.2	94.1

Table 7: Quantitative evaluation on RGB-D frames from ICL-NUIM "Living Room" sequence. The best result is in bold, the second best is underlined.

Office																	
	RMSE <sub>d</sub>		BadPix <sub>d</sub> (5cm)		BadPix <sub>v</sub> (5)		DSSIM <sub>v</sub>		LPIPS <sub>v</sub>		Bumpiness <sub>d</sub>		RMSE <sub>v</sub>		User, 1st	User, 2nd	Top 2
	x4	x8	x4	x8	x4	x8	x4	x8	x4	x8	x4	x8	x4	x8	x4	x4	x4
Bicubic	47	80	4.0	7.8	<u>24.4</u>	<u>34.1</u>	<u>216</u>	<u>285</u>	<u>412</u>	<u>594</u>	0.81	0.95	208	254	<u>19.9</u>	<b>44.1</b>	<u>64.0</u>
SRfS [14]	49	89	5.8	14.4	53.4	54.4	595	593	690	636	1.71	1.66	298	302	0.0	0.0	0.0
PDN [39]	185	185	99.3	90.5	36.5	50.2	250	294	457	518	<u>0.76</u>	<u>0.92</u>	234	272	0.7	3.7	4.4
DG [13]	49	85	9.0	11.9	36.5	37.6	319	330	534	571	1.03	1.05	240	266	0.0	0.7	0.7
DIP [47]	76	109	30.3	48.2	72.1	73.9	726	819	690	797	2.45	2.70	372	408	1.5	1.5	2.9
MSG [22]	<u>35</u>	<b>48</b>	2.4	6.8	35.4	44.5	263	360	415	543	0.83	0.95	199	247	2.2	3.7	5.9
DIP-v	40	<u>65</u>	3.8	7.4	45.4	47.9	311	352	414	<u>504</u>	1.08	1.18	205	<u>235</u>	17.6	<u>25.0</u>	42.6
MSG-v	<b>32</b>	<u>65</u>	<b>1.9</b>	<b>5.3</b>	<b>19.3</b>	<b>29.6</b>	<b>157</b>	<b>224</b>	<b>313</b>	<b>432</b>	<b>0.59</b>	<b>0.72</b>	<b>151</b>	<b>198</b>	<b>58.1</b>	21.3	<b>79.4</b>
Coat rack																	
Bicubic	<u>13</u>	20	1.5	3.0	<u>73.1</u>	<u>75.3</u>	<u>507</u>	539	537	651	0.54	0.60	171	196	0.0	<u>19.1</u>	19.1
SRfS [14]	24	28	3.8	5.4	82.3	80.5	672	556	650	612	0.83	0.57	237	203	0.0	0.0	0.0
EG [54]	<u>13</u>		1.2		77.8		541		550		0.55		186		0.7	7.4	8.1
PDN [39]	140	191	99.6	99.9	77.1	78.0	544	557	621	631	<u>0.48</u>	<u>0.50</u>	178	193	<u>5.1</u>	<b>28.7</b>	<u>33.8</u>
DG [13]	<u>13</u>	20	1.4	3.2	74.4	75.6	530	<u>532</u>	593	621	0.54	0.58	166	201	0.0	9.6	9.6
DIP [47]	15	24	1.9	3.5	85.5	85.4	766	701	625	624	1.15	0.97	256	246	4.4	2.2	6.6
MSG [22]	<b>11</b>	<b>17</b>	<u>0.9</u>	<b>1.6</b>	73.3	76.1	522	546	523	<u>554</u>	0.51	0.55	<u>165</u>	189	2.2	16.2	18.4
DIP-v	<u>13</u>	<b>17</b>	1.8	<u>2.0</u>	75.2	75.5	543	542	<b>422</b>	<b>463</b>	0.62	0.60	171	<u>181</u>	0.7	12.5	13.2
MSG-v	<b>11</b>	<u>18</u>	<b>0.8</b>	2.2	<b>71.4</b>	<b>74.2</b>	<b>482</b>	<b>502</b>	<u>516</u>	563	<b>0.42</b>	<b>0.48</b>	<b>136</b>	<b>161</b>	<b>86.8</b>	4.4	<b>91.2</b>
Displays																	
Bicubic	41	63	3.2	6.4	49.9	<u>54.9</u>	<u>315</u>	<u>374</u>	460	585	0.92	1.08	208	256	0.7	<u>21.3</u>	22.1
SRfS [14]	53	75	9.0	17.3	61.9	67.3	500	591	599	659	1.35	1.60	288	328	0.0	0.0	0.0
EG [54]	46		5.9		66.7		388		587		0.94		216		0.0	2.9	2.9
PDN [39]	159	220	99.2	99.0	55.4	57.2	381	403	547	580	<u>0.85</u>	<u>0.95</u>	242	275	0.0	9.6	9.6
DG [13]	43	66	5.8	6.7	56.5	56.7	395	406	606	601	1.06	1.10	243	265	0.7	2.9	3.7
DIP [47]	52	60	13.4	9.7	76.9	74.6	732	724	672	645	2.36	2.06	365	344	0.7	0.7	1.5
MSG [22]	<u>26</u>	<b>42</b>	<u>1.7</u>	4.4	53.9	58.0	367	430	461	<u>493</u>	0.97	1.08	204	251	0.0	5.9	5.9
DIP-v	32	45	2.4	4.0	53.7	57.6	336	407	<b>344</b>	<b>409</b>	1.00	1.18	<u>191</u>	<u>221</u>	<u>5.9</u>	<b>51.5</b>	<u>57.4</u>
MSG-v	<b>23</b>	<u>43</u>	<b>1.4</b>	<b>3.5</b>	<b>47.2</b>	<b>51.0</b>	<b>271</b>	<b>324</b>	<u>451</u>	531	<b>0.69</b>	<b>0.80</b>	<b>152</b>	<b>190</b>	<b>91.9</b>	5.1	<b>97.1</b>

Table 8: Quantitative evaluation on RGB-D frames from ICL-NUIM "Office Room" sequence. The best result is in bold, the second best is underlined.

Vintage																	
	RMSE <sub>d</sub>		BadPix <sub>d</sub> (5cm)		BadPix <sub>v</sub> (5)		DSSIM <sub>v</sub>		LPIPS <sub>v</sub>		Bumpiness <sub>d</sub>		RMSE <sub>v</sub>		User, 1st	User, 2nd	Top 2
	x4	x8	x4	x8	x4	x8	x4	x8	x4	x8	x4	x8	x4	x8	x4	x4	x4
Bicubic	67	98	4.6	9.0	72.8	<b>77.3</b>	558	649	602	729	1.51	1.64	258	302	5.9	28.7	34.6
SRfS [14]	101	145	16.8	32.3	83.7	87.2	721	749	631	634	1.64	1.68	346	382	0.0	0.0	0.0
PDN [39]	140	174	67.6	79.0	82.3	85.7	663	714	706	700	1.51	1.57	319	350	0.0	0.0	0.0
DG [13]	72	107	7.1	10.4	79.4	80.1	666	669	796	840	1.50	1.52	290	300	0.0	0.7	0.7
DIP [47]	74	117	24.8	46.9	93.6	94.2	953	965	910	872	4.01	4.16	656	687	0.7	0.7	1.5
MSG [22]	41	59	3.2	6.8	80.6	84.6	708	785	510	610	1.62	1.85	292	364	0.0	9.6	9.6
DIP-v	42	67	2.7	5.9	85.2	88.8	804	884	579	674	1.94	2.48	343	435	25.7	44.1	69.9
MSG-v	33	65	2.5	5.9	71.4	77.6	536	643	670	702	1.29	1.43	211	268	67.6	16.2	83.8
Recycle																	
Bicubic	587	880	9.2	16.6	70.6	78.6	575	721	474	576	1.23	1.17	329	398	0.0	11.0	11.0
SRfS [14]	47	72	10.2	22.1	86.1	88.8	715	772	610	623	1.68	1.81	376	410	0.0	0.0	0.0
PDN [39]	95	128	90.5	79.8	84.0	85.7	635	701	523	589	1.66	2.18	364	457	0.0	6.6	6.6
DG [13]	39	82	3.4	11.7	81.6	83.6	696	719	602	617	1.75	1.99	328	383	2.9	65.4	68.4
DIP [47]	29	45	3.9	9.3	91.0	91.8	871	923	576	605	2.95	3.31	434	500	1.5	5.9	7.4
MSG [22]	106	1182	5.8	11.9	82.8	89.6	741	869	624	661	2.60	3.01	485	550	0.7	0.0	0.7
DIP-v	20	34	1.5	4.2	78.9	85.0	575	735	388	485	1.56	1.86	273	332	94.9	3.7	98.5
MSG-v	51	76	3.9	7.9	73.9	82.1	603	737	520	564	1.66	2.02	368	473	0.0	7.4	7.4

Table 9: Quantitative evaluation on samples with small number of missing measurements from Middlebury dataset. The best result is in bold, the second best is underlined.

Umbrella																	
	RMSE <sub>d</sub>		BadPix <sub>d</sub> (5cm)		BadPix <sub>v</sub> (5)		DSSIM <sub>v</sub>		LPIPS <sub>v</sub>		Bumpiness <sub>d</sub>		RMSE <sub>v</sub>		User, 1st	User, 2nd	Top 2
	x4	x8	x4	x8	x4	x8	x4	x8	x4	x8	x4	x8	x4	x8	x4	x4	x4
Bicubic	1013	1507	6.9	12.1	<b>77.7</b>	<b>80.9</b>	<b>749</b>	837	747	886	<b>0.60</b>	<b>0.60</b>	<u>323</u>	<u>380</u>	<u>5.9</u>	<b>35.3</b>	<u>41.2</u>
SRfS [14]	148	217	19.4	35.5	87.5	90.8	843	853	797	831	0.71	<u>0.78</u>	397	443	0.0	0.0	0.0
PDN [39]	220	287	94.9	89.1	86.6	88.1	799	<b>828</b>	847	882	0.79	1.13	367	452	3.7	<u>22.8</u>	26.5
DG [13]	365	507	9.1	20.3	84.6	87.3	846	878	781	856	0.92	1.36	399	457	0.0	0.7	0.7
DIP [47]	138	<u>145</u>	48.5	21.6	90.5	93.2	915	953	737	<u>722</u>	1.19	1.65	467	528	2.9	16.2	19.1
MSG [22]	292	555	7.4	12.4	84.3	88.1	834	896	<u>678</u>	787	1.27	1.47	442	496	0.0	0.7	0.7
DIP-v	<b>91</b>	<b>129</b>	<b>3.4</b>	<b>5.7</b>	83.4	85.3	796	854	<b>604</b>	<b>598</b>	<u>0.67</u>	0.79	<b>318</b>	<b>352</b>	<b>82.4</b>	8.1	<b>90.4</b>
MSG-v	<u>129</u>	218	<u>5.2</u>	<u>9.7</u>	<u>79.1</u>	<u>82.3</u>	<u>778</u>	842	800	890	0.72	0.89	348	427	5.1	16.2	21.3
Classroom1																	
Bicubic	966	1371	6.7	<u>9.0</u>	<b>75.8</b>	<b>78.3</b>	<b>636</b>	<b>728</b>	<u>581</u>	784	<b>0.41</b>	<b>0.30</b>	<u>268</u>	<b>295</b>	12.5	<b>37.5</b>	<u>50.0</u>
SRfS [14]	135	202	18.5	28.5	82.6	85.7	761	781	718	756	0.62	0.62	332	363	0.0	0.0	0.0
PDN [39]	239	324	96.0	91.0	81.5	82.9	739	759	751	807	0.62	0.76	279	342	<u>16.9</u>	<u>26.5</u>	43.4
DG [13]	307	503	8.8	16.8	82.0	82.7	743	762	766	812	0.74	0.87	313	337	0.0	1.5	1.5
DIP [47]	<u>96</u>	<u>145</u>	17.0	22.4	94.4	94.6	956	952	789	751	1.94	2.12	540	557	0.0	1.5	1.5
MSG [22]	297	408	7.3	10.0	81.2	83.8	723	810	626	<u>604</u>	0.90	1.01	351	391	0.0	0.7	0.7
DIP-v	<b>69</b>	<b>117</b>	<b>4.1</b>	9.3	81.0	86.0	700	789	<b>516</b>	<b>537</b>	0.64	0.86	<b>266</b>	<u>327</u>	<b>64.0</b>	18.4	<b>82.4</b>
MSG-v	127	203	<u>5.4</u>	<b>8.4</b>	<u>76.9</u>	<u>79.4</u>	<u>678</u>	<u>735</u>	739	803	<u>0.60</u>	0.64	283	330	2.2	11.8	14.0

Table 10: Quantitative evaluation on samples with small number of missing measurements from Middlebury dataset. The best result is in bold, the second best is underlined.

Playroom																	
	RMSE <sub>d</sub>		BadPix <sub>d</sub> (5cm)		BadPix <sub>v</sub> (5)		DSSIM <sub>v</sub>		LPIPS <sub>v</sub>		Bumpiness <sub>d</sub>		RMSE <sub>v</sub>		User, 1st	User, 2nd	Top 2
	x4	x8	x4	x8	x4	x8	x4	x8	x4	x8	x4	x8	x4	x8	x4	x4	x4
Bicubic	1263	1744	14.4	20.4	<b>72.0</b>	<b>76.9</b>	<b>684</b>	<b>783</b>	<u>509</u>	675	<b>0.80</b>	<b>0.52</b>	<u>386</u>	<u>441</u>	0.0	2.2	2.2
SRfS [14]	97	151	26.9	42.1	88.1	91.2	802	829	663	715	<u>1.24</u>	<u>1.08</u>	493	540	0.0	0.0	0.0
PDN [39]	181	253	85.0	69.7	86.3	89.2	820	862	583	656	1.54	1.88	472	543	<u>25.7</u>	<b>61.8</b>	<u>87.5</u>
DG [13]	425	133	22.4	25.0	85.4	86.0	845	826	779	691	1.96	1.63	519	469	1.5	2.2	3.7
DIP [47]	<u>58</u>	<u>91</u>	18.4	20.0	93.0	93.2	941	937	647	<u>612</u>	3.09	2.86	602	592	1.5	2.9	4.4
MSG [22]	433	349	16.1	22.3	85.8	89.9	855	911	685	705	2.51	2.74	576	616	0.0	0.0	0.0
DIP-v	<b>49</b>	<b>83</b>	<b>5.4</b>	<b>12.2</b>	83.8	88.5	728	847	<b>459</b>	<b>530</b>	1.29	1.52	<b>357</b>	<b>433</b>	<b>70.6</b>	<u>27.2</u>	<b>97.8</b>
MSG-v	112	166	<u>9.4</u>	<u>15.5</u>	<u>75.2</u>	<u>80.1</u>	<u>721</u>	810	565	615	1.46	1.67	453	510	0.0	3.7	3.7
Backpack																	
Bicubic	985	1078	14.3	11.5	<b>62.7</b>	<b>69.4</b>	<b>639</b>	<b>730</b>	<u>564</u>	692	<b>0.60</b>	<b>0.45</b>	<b>392</b>	<b>424</b>	2.2	<u>34.6</u>	36.8
SRfS [14]	69	83	18.9	25.5	89.9	89.9	831	847	630	651	1.37	1.26	500	505	0.0	0.0	0.0
PDN [39]	173	207	81.6	65.2	80.4	85.4	770	820	609	719	1.59	1.96	519	553	<u>3.7</u>	<b>37.5</b>	<u>41.2</u>
DG [13]	325	465	26.5	39.9	77.0	82.0	765	808	650	696	1.62	2.07	529	545	0.7	2.9	3.7
DIP [47]	<u>41</u>	<u>67</u>	<u>8.2</u>	17.9	93.2	94.5	943	984	766	692	3.36	2.95	639	645	1.5	11.8	13.2
MSG [22]	211	170	15.1	<u>10.4</u>	76.5	86.9	762	856	671	723	2.11	2.31	577	609	0.7	0.0	0.7
DIP-v	<b>38</b>	<b>62</b>	<b>6.2</b>	12.9	82.5	88.7	677	768	<b>457</b>	<b>496</b>	1.31	1.43	<u>409</u>	<u>448</u>	<b>90.4</b>	5.1	<b>95.6</b>
MSG-v	113	89	10.8	<b>5.9</b>	<u>65.3</u>	<u>72.5</u>	<u>663</u>	<u>752</u>	<u>577</u>	<u>635</u>	<u>1.07</u>	<u>1.15</u>	462	480	0.0	5.9	5.9
Jadeplant																	
Bicubic	1017	1297	19.3	18.4	<b>68.8</b>	<b>75.7</b>	<u>695</u>	<u>788</u>	<u>545</u>	696	<b>0.97</b>	<b>0.62</b>	<b>449</b>	<b>464</b>	2.3	<u>27.7</u>	30.0
SRfS [14]	105	143	39.5	48.9	87.2	92.7	787	839	637	719	1.96	1.70	551	583	0.0	0.0	0.0
PDN [39]	161	205	81.8	62.0	82.4	88.0	778	849	551	<u>625</u>	1.95	2.20	512	572	<u>19.1</u>	<b>41.4</b>	<u>60.5</u>
DG [13]	326	512	27.8	47.6	82.6	86.8	791	823	718	670	2.28	2.66	567	601	0.0	0.5	0.5
DIP [47]	<b>70</b>	<u>121</u>	<u>16.7</u>	32.8	91.2	92.3	913	911	735	764	3.19	3.21	615	638	0.0	0.5	0.5
MSG [22]	216	263	21.1	<u>17.8</u>	81.5	87.6	796	880	751	783	2.73	2.90	614	649	0.0	0.0	0.0
DIP-v	<u>84</u>	<u>121</u>	21.8	24.0	86.6	89.5	820	870	<b>542</b>	654	1.92	1.99	<u>503</u>	<u>535</u>	<b>78.2</b>	20.5	<b>98.6</b>
MSG-v	109	<b>117</b>	<b>13.9</b>	<b>11.2</b>	<u>71.0</u>	<u>79.0</u>	<b>688</b>	<b>781</b>	605	<b>622</b>	<u>1.61</u>	<u>1.66</u>	507	<u>529</u>	0.5	8.2	8.6

Table 11: Quantitative evaluation on samples with large number of missing measurements from Middlebury dataset. The best result is in bold, the second best is underlined.